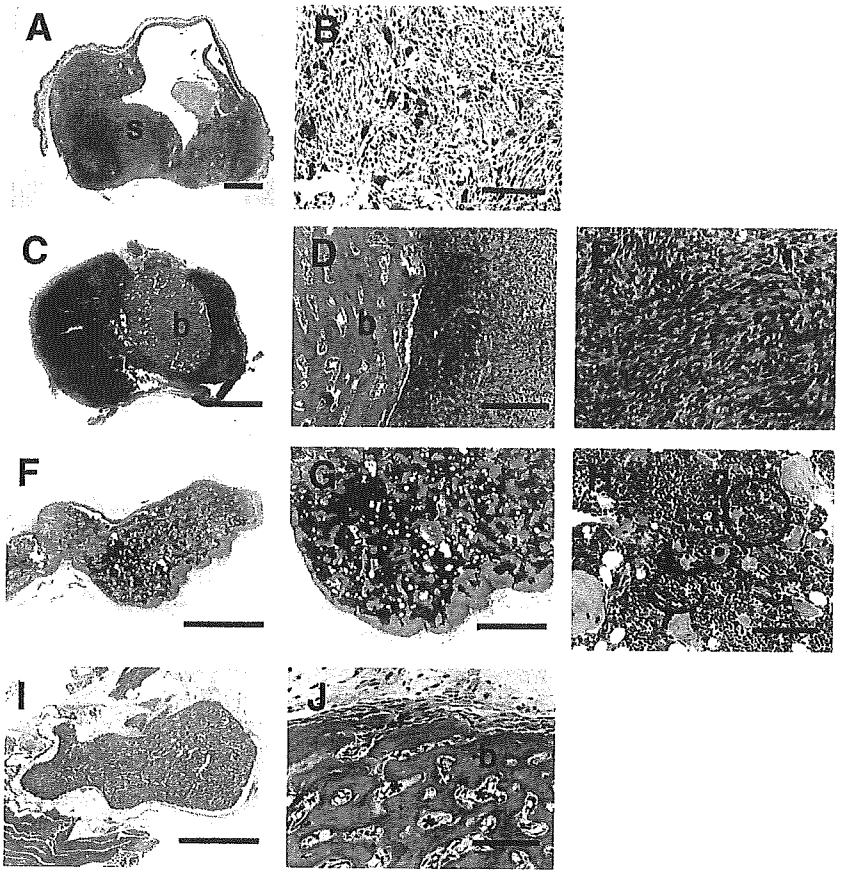

Fig. 5. Microscopic appearance of subcutaneous masses 4 weeks after subcutaneous inoculation of NIH3T3-MTAg (A, B), KUSA-MTAg (C, D, E), KUSA (F, G, H), and KUSA-A1 cells (I, J). (A) Mass of the first type. It is a sarcoma [s] without bone. (B) High-power view of a part of panel (A). The tumor consists of pleomorphic mesenchymal cells, including multinucleated bizarre giant cells. (C, D) Mass of the second type. The mass is composed of sarcoma [s] and well-defined bone [b]. (E) High-power view of part of the tumor in panel (D). The tumor shows proliferation of pleomorphic spindle cells, including giant multinucleated tumor cells. (F, G) Mass of the third type. The mass is composed of complete bone with bone cavities [asterisks], but there is no sarcomatous proliferation. (H) High-power view of part of the mass in panel (G). Trilineage hematopoietic cells (granulocytes [g], erythrocytes [e], and megakaryocyte [arrow]) in the bone cavities inside the mass are shown. (I) Mass of the third type. The mass is composed of complete bone with bone cavities [asterisks], but there is sarcomatous proliferation. (J) High-power view of panel (I). H–E stain. Scale bars: 2 mm (A, C, F, K), 0.5 mm (G), 200 μm (D), and 100 μm (B, E, H, J).

Histological examination of complete bone mass revealed highly dense bone trabeculae, and hematopoietic cells were observed in the bone marrow, as reported previously [6,10]. No cartilage had formed in any of the KUSA-A1-produced bones, indicating that the osteogenesis by KUSA-A1 is membranous ossification rather than enchondral ossification. Osteogenesis was monitored radiographically at scheduled times after the inoculation of $3-5 \times 10^7$ KUSA-A1 cells, and the results showed a gradual increase in newly formed bone 2 weeks after the injection, and complete bone density 4 weeks after the inoculation.

We then monitored the fate of KUSA-A1 bone transplanted into subcutaneous tissue and the abdominal cavity and found that the ectopic KUSA-A1 bone remained unchanged in size and shape for 12 months at both sites. Histological examination revealed complete functional hematopoiesis by ectopic KUSA-A1 bone in the subcutaneous tissue, but not in the abdominal cavity.

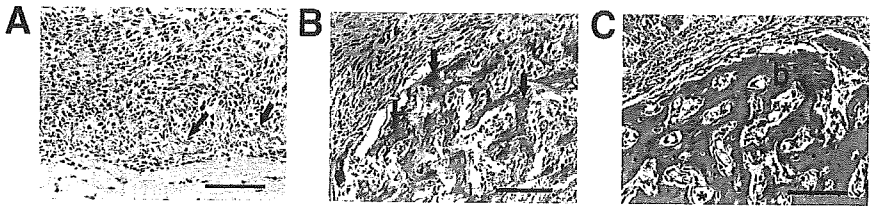

Fig. 6. The process of osteogenesis by KUSA-A1 cells in vivo. (A) One week after the inoculation of 10^7 KUSA-A1 cells, bone formation [arrows] was observed around the periphery of the mass at all inoculation sites. It is noteworthy that no chondrogenesis was observed during early osteogenesis. (B) Two weeks after inoculation. There is more bone matrix [arrows] at week 2 than at week 1. (C) Four weeks after inoculation, the mass consists of complete bone tissue [b] and bone cavities [asterisks]. H–E stain. Scale bars: 100 μm.

4. Discussion

4.1. KUSA-A1 cells can be used as a model for developmental bone formation and abnormal ossification

The sequence of KUSA-A1 bone formation is as follows: deposition of matrix by KUSA-A1 cells that subsequently become mineralized, deposition of bone as a network of immature or woven trabeculae, and formation of bone marrow or conversion of the spongiosa into primary cortical bone by filling of spaces between the trabeculae. This process results in the formation of cancellous bone and bone marrow. Importantly, the osteogenesis by KUSA-A1 cells was irreversible and reproducible, and the transplanted KUSA-A1 cells never transformed into malignant cells, formed any abnormal extracellular matrices, or induced any significant inflammatory reactions. It is noteworthy that the osteogenesis by KUSA-A1 cells was not mediated by chondrogenesis, and it was therefore considered to be membranous ossification. Thus, the unique characteristics of KUSA-A1 cells provide an opportunity to analyze the process of membranous ossification in an experimental system in detail.

In fetal life, primary ossification centers form by one of two processes: endochondral ossification or membranous ossification. Endochondral ossification refers to bony replacement of cartilage and is the mode of formation of the long bones. During membranous ossification, mesenchymal cells form membranes within which ossification occurs, and this is the mode of formation of the scapula and skull and, in part, of the clavicle and pelvis. After birth, bone growth continues by both endochondral and membranous ossification. Further endochondral ossification occurs in the physes and results in continuous longitudinal growth of the long bones until skeletal maturity. KUSA-A1 cells were obtained from a long bone the femur, but formed bone by membranous ossification. There are also cells responsible for the periosteal membranous ossification in tubular bones, which model the diaphyseal cortex, and KUSA-A1 cells may be derived from such a minor cell population in long bones that is responsible for periosteal bone formation or callus.

The process of ossification by KUSA-A1 cells may also serve a model for ectopic or heterotopic ossification, such as soft tissue ossification, ligament ossification, and heterotopic bone formation in a number of disorders, including central nervous system and spinal cord disorders, probably as a consequence of immobilization, a model of myositis ossificans progressiva, which often develops after a traumatic event, and a model of ossification of the posterior longitudinal ligament of the spine, which is characterized by the presence of a linear band of ossification along the posterior margin of vertebral bodies and intervertebral discs, especially in the cervical spine.

4.2. Possibility of implanted-cell transformation

The lack of tumor formation or in vivo transformation after implantation of KUSA-A1 cells into immunodeficient mice does not mean that the donor cells are incapable of transforming after implantation, at least in mice. The observation period after cell implantation into mice is usually less than 1 year because the life span of mice is approximately 2 years. By contrast, since patients who receive cell-based therapy may survive for decades, the possibility of implanted-cell transformation cannot be ignored. Care should be exercised when using donor cells transfected with certain genes for the therapeutic purposes, because zero risk of implanted-cell transformation cannot be achieved, even though human non-tumor cells seldom transform in vitro or in vivo without gene transfection.

4.3. Can cancellous bone grafting be replaced by osteoblast-based therapy?

The transplantation of bone from one site to another usually promotes osteogenesis or provides structural stability. Grafts may be used to fill bone defects, promote union, or provide material for arthrodesis. The donor sites most frequently used for grafts are the iliac crest, tibia, and fibula. Depending on circumstances, the patient or animal may receive either a cancellous bone graft or a cortico-cancellous graft. Cancellous bone grafts are the gold standard for bone defects. They have greater capacity to induce new bone formation and, thus, are considered to be generally much more successful in inducing new bone formation than osteoblast-based therapy. Osteoblast-based therapy is poorer than cancellous bone grafts in providing structural stability.

However, complications occur after cancellous bone grafting and include fracture at the donor site, intraoperative bleeding, and postoperative pain. Graft failure may lead to progressive bone resorption and, ultimately, to disappearance of the graft. Follow-up radiographs show healing of iliac donor sites with sclerosis at the margins of the bone defects. Painful excrescences of the bone may develop at the donor site. Loss of the sharp margins between the graft and host bone on radiographs generally signifies graft healing, and the persistence of a thin residual radiolucent area between the graft and the host bone suggests fibrous union.

It would be interesting to assess the possibility of using mature osteoblasts as a therapeutic agent. The inoculation of isolated mature osteoblasts into a bone defect or fracture site would be a more efficient means of accelerating bone fusion with minimal invasion than inoculation of unfractionated marrow cells into fracture sites. The critical step in realizing osteoblast-based therapy will be the isolation of human counterparts to KUSA-A1 cells and growing them in sufficient numbers in culture. The separation of osteoblasts from human marrow stroma [21] and inoculation of the cells with an appropriate scaffold will provide new methods of

osteogenesis engineering without any of the complications associated with cancellous bone grafts.

Acknowledgements

We would like to express our sincere thanks to Y. Takeda and H. Abe for support throughout the work, and to N. Hida, T. Inomata, Y. Hashimoto, and Y. Nakamura, for providing expert technical assistance. This study was supported by a grant from the Ministry of Education, Culture, Sports, Science, and Technology of Japan, the Health and Labour Sciences Research Grants, and the Pharmaceuticals and Medical Devices Agency to A. U.

References

[1] P. Bianco, P.G. Robey, Marrow stromal stem cells, J. Clin. Invest. 105 (2000) 1663–1668.
[2] M.C. Horowitz, A. Fields, D. DeMeo, H.Y. Qian, A.L. Bothwell, E. Trepman, Expression and regulation of Ly-6 differentiation antigens by murine osteoblasts, Endocrinology 135 (1994) 1032–1043.
[3] E. Canalis, Novel treatments for osteoporosis, J. Clin. Invest. 106 (2000) 177–179.
[4] G.A. Rodan, T.J. Martin, Therapeutic approaches to bone diseases, Science 289 (2000) 1508–1514.
[5] M.F. Pittenger, A.M. Mackay, S.C. Beck, R.K. Jaiswal, R. Douglas, J.D. Mosca, M.A. Moorman, D.W. Simonetti, S. Craig, D.R. Marshak, Multilineage potential of adult human mesenchymal stem cells, Science 284 (1999) 143–147.
[6] A. Umezawa, T. Maruyama, K. Segawa, R.K. Shadduck, A. Waheed, J. Hata, Multipotent marrow stromal cell line is able to induce hematopoiesis in vivo, J. Cell. Physiol. 151 (1992) 197–205.
[7] S. Makino, K. Fukuda, S. Miyoshi, F. Konishi, H. Kodama, J. Pan, M. Sano, T. Takahashi, S. Hori, H. Abe, J. Hata, A. Umezawa, S. Ogawa, Cardiomyocytes can be generated from marrow stromal cells in vitro, J. Clin. Invest. 103 (1999) 697–705.
[8] S. Gojo, N. Gojo, Y. Takeda, T. Mori, H. Abe, S. Kyo, J. Hata, A. Umezawa, In vivo cardiovasculogenesis by direct injection of isolated adult mesenchymal stem cells, Exp. Cell Res. 288 (2003) 51–59.
[9] J. Kohyama, H. Abe, T. Shimazaki, A. Koizumi, K. Kashima, S. Gojo, T. Taga, H. Okano, J. Hata, A. Umezawa, Brain from bone: efficient 'meta-differentiation' of marrow stroma-derived mature osteoblasts to neurons with Noggin or a demethylating agent, Differentiation 68 (2001) 235–244.
[10] K. Ochi, G. Chen, T. Ushida, S. Gojo, K. Segawa, H. Tai, K. Ueno, H. Ohkawa, T. Mori, A. Yamaguchi, Y. Toyama, J. Hata, A. Umezawa, Use of isolated mature osteoblasts in abundance acts as desired-shaped bone regeneration in combination with a modified poly-DL-lactic-co-glycolic acid (PLGA)-collagen sponge, J. Cell. Physiol. 194 (2003) 45–53.
[11] A. Sharov, et al., Transcriptome analysis of mouse stem cells and early embryos, PLoS Biol. 1 (2003) E74.
[12] A. Umezawa, K. Harigaya, H. Abe, Y. Watanabe, Gap-junctional communication of bone marrow stromal cells is resistant to irradiation in vitro, Exp. Hematol. 18 (1990) 1002–1007.
[13] A. Umezawa, J. Hata, Expression of gap-junctional protein (connexin 43 or alpha 1 gap junction) is down-regulated at the transcriptional level during adipocyte differentiation of H-1/A marrow stromal cells, Cell Struct. Funct. 17 (1992) 177–184.
[14] A. Umezawa, K. Tachibana, K. Harigaya, S. Kusakari, S. Kato, Y. Watanabe, T. Takano, Colony-stimulating factor 1 expression is down-regulated during the adipocyte differentiation of H-1/A marrow stromal cells and induced by cachectin/tumor necrosis factor, Mol. Cell. Biol. 11 (1991) 920–927.
[15] H. Sudo, A. Kodama, Y. Amagai, S. Yamamoto, S. Kasai, In vitro differentiation and calcification in a new clonal osteogenic cell line derived from newborn mouse calvaria, J. Cell Biol. 96 (1983) 191–198.
[16] S.B. Doty, B.H. Schofield, Enzyme histochemistry of bone and cartilage cells, Prog. Histochem. Cytochem. 8 (1976) 1–38.
[17] I. Binderman, D. Duksin, A. Harell, E. Katzir, L. Sachs, Formation of bone tissue in culture from isolated bone cells, J. Cell Biol. 61 (1974) 427–439.
[18] P.C. Schiller, G. D'Ippolito, W. Balkan, B.A. Roos, G.A. Howard, Gap-junctional communication is required for the maturation process of osteoblastic cells in culture, Bone 28 (2001) 362–369.
[19] M.M. Saunders, J. You, J.E. Trosko, H. Li, Z. Yamasaki, H.J. Donahue, C.R. Jacobs, Gap junctions and fluid flow response in MC3T3-E1 cells, Am. J. Physiol., Cell Physiol. 281 (2001) C191725.
[20] P.S. Leboy, J.N. Beresford, C. Devlin, M.E. Owen, Dexamethasone induction of osteoblast mRNAs in rat marrow stromal cell cultures, J. Cell. Physiol. 146 (1991) 370–378.
[21] T. Mori, T. Kiyono, H. Imabayashi, Y. Takeda, K. Tsuchiya, S. Miyoshi, H. Makino, H. Matsumoto, H. Saito, S. Ogawa, M. Sakamoto, J-i Hata, A. Umezawa, Combination of hTERT and Bmi-1, E6 or E7 induce prolongation of the life span of bone marrow stromal cells from an elderly donor without affecting their neurogenic potential, Mol. Cell. Biol. 25 (2005) 5183–5195.

Laboratory Investigation (2005) 85, 1210–1223

www.laboratoryinvestigation.org

Interleukin-6/soluble interleukin-6 receptor complex reduces infarct size via inhibiting myocardial apoptosis

Kenichi Matsushita[1], Shiro Iwanaga[1], Takahiro Oda[1], Kensuke Kimura[1], Megumi Shimada[1], Makoto Sano[2], Akihiro Umezawa[2,*], Jun-ichi Hata[2,†] and Satoshi Ogawa[1]

[1]*Cardiopulmonary Division, Department of Medicine, Keio University School of Medicine, Shinjuku-ku, Tokyo, Japan and* [2]*Department of Pathology, Keio University School of Medicine, Shinjuku-ku, Tokyo, Japan*

Apoptosis of cardiomyocytes plays an important role in reperfusion injury following myocardial infarction. Conversely, interleukin-6 (IL-6)—a potent cytokine—inhibits myeloma cell apoptosis by activating GP130 through the IL-6 receptor (IL-6R). We hypothesized that the IL-6/soluble IL-6R complex can inhibit myocardial apoptosis, and limit infarct size in reperfused acute myocardial infarction. Anesthetized rats were randomly divided into five groups: sham, coronary occlusion and reperfusion rats administered IL-6/soluble IL-6R complex, IL-6 alone, soluble IL-6R (sIL-6R) alone, or a control vehicle. Rats were subjected to 30 min occlusion of the left coronary artery followed by 3 h reperfusion. After reperfusion, the hearts were excised. For detection and quantification of apoptosis, gel electrophoresis of extracted genomic DNA and TUNEL method of paraffin sections were performed. The percentage of the infarct area was measured using tetrazolium chloride staining. The cardiomyocyte apoptosis analysis revealed that apoptosis in the reperfused myocardium was inhibited only in the complex group. Furthermore, the percentage of the infarct area out of the area at risk was remarkably reduced in the complex group (23.8±1.8%), compared with that in the vehicle (37.9±3.7%), the IL-6 (40.7±1.0%), or the sIL-6R (37.5±2.4%) groups ($P=0.0002$). No significant differences were observed among the vehicle, IL-6, and sIL-6R groups. The IL-6/soluble IL-6 receptor complex inhibits cardiomyocyte apoptosis in reperfused acute myocardial infarction. It possibly reduces irreversible reperfusion injury.
Laboratory Investigation (2005) **85,** 1210–1223. doi:10.1038/labinvest.3700322; published online 1 August 2005

Keywords: apoptosis; gp130; interleukin-6; myocardial infarction; reperfusion

Interleukin-6/soluble interleukin-6 receptor (IL-6/sIL-6R) complex exhibits various functions in the central nervous system, the hematopoietic system, and other tissues.[1–6] Classically, many soluble receptors are used to inhibit ligand signaling of the native receptor.[7] However, soluble IL-6R acts as an agonist of IL-6 activity. The receptor for IL-6 is composed of two distinct membrane-bound glycoproteins, an 80 kDa cognate receptor subunit (IL-6R) and a 130 kDa signal-transducing element (gp130).[8–11] The binding of IL-6 to the IL-6R induces the homodimerization of gp130. Homodimerisation of the two gp130 molecules causes phosphorylation of gp130 and the transcription factors STAT1 and STAT3 by Janus-Kinases (JAK1, JAK2, TYK2), which are constitutively associated with gp130.[12] Neither IL-6 nor IL-6R alone binds or activates gp130. The heterodimeric complex IL-6/ IL-6R acts as the active cytokine.[6] A soluble form of the IL-6R (sIL-6R) is still able to bind IL-6 and the complex of IL-6 and the sIL-6R activates target cells expressing gp130. In IL-6 signaling, the activation of STAT3 was shown to be linked with antiapoptotic signals through the induction of bcl-2.[13] Furthermore, IL-6 was reported to inhibit apoptosis of malignant plasma cells,[14] which express IL-6 receptors.[15,16] In target cells expressing membrane-bound IL-6R, the function of IL-6 is further augmented by the addition of sIL-6R.[17,18] In target cells expressing a small or no available number of membrane-bound IL-6R but expressing gp130, exogenously added IL-6 fail to exert its functions; however, coadministration of soluble IL-6R with IL-6 induces IL-6-mediated functions.[1,5]

Correspondence: Dr S Iwanaga, MD, PhD, Cardiopulmonary Division, Department of Medicine, Keio University School of Medicine, 35 Shinanomachi, Shijuku-ku, Tokyo 160-8582, Japan. E-mail: siwanaga@sc.itc.keio.ac.jp

*Present address: National Research Institute for Child Health and Development, Tokyo 157-8535, Japan.

†Present address: National Center for Child Health and Development, Tokyo 157-8535, Japan.

Received 6 January 2005; revised 18 May 2005; accepted 6 June 2005; published online 1 August 2005

Although gp130 is expressed on cardiomyocytes,[9,19] whether cardiomyocytes express IL-6R is controversial. Saito *et al*[9] reported that cardiomyocytes did not express IL-6R, while Youker *et al* showed that IL-6 activated IL-6 signal pathway in cardiomyocytes.[20] Chandrasekar *et al*[21] did not detect IL-6R mRNA in control myocardium, but found its upregulation in ischemic/reperfused myocardium. To examine whether IL-6 signaling inhibits apoptosis of cardiomyocyte as well as myeloma cells, a rat myocardial ischemia/reperfusion model, in which apoptosis of cardiomyocytes has previously been documented,[22] was used in this investigation.

Clinically, the mainstay of treatment for acute myocardial infarction has strived to decrease the amount of infarcted myocardium. This has involved timely intervention by reperfusion of the occluded coronary artery; early reperfusion techniques include primary angioplasty and thrombolytic therapy.[23] However, the apparent protective effect of timely reperfusion in acute myocardial infarction is accompanied by a paradoxical acceleration in residual cell death of the reperfused myocardium. These potential deleterious effects of reperfusion on the myocardium constitute the dilemma of reperfusion injury.[24,25] The precise mechanism of reperfusion injury remains to be elucidated; however, myocardial apoptosis has been thought to contribute significantly to reperfusion injury.[22,26,27] Optimizing the process of reperfusion to reduce these deleterious effects, perhaps by the administration of adjunctive therapies or by altering the myocardial environment, could further improve the outcome of clinical intervention.[28,29]

In the present study, we showed that IL-6/sIL-6R complex, but not IL-6 or sIL-6R alone, inhibited myocardial apoptosis in reperfused acute myocardial infarction. We further showed that IL-6/sIL-6R complex reduced infarct size in this model.

Materials and methods

Experimental Protocols

Human recombinant IL-6 was obtained from INTERGEN (New York, USA). Human sIL-6R was generously provided by Dr Tadamitsu Kishimoto of Osaka University. Human sIL-6R has been purified from human serum and urine.[8,17,30] This soluble receptor binds IL-6 with an affinity similar to that of the cognate receptor (0.5–2 nM)[31,32] and prolongs its plasma half-life.[8,33] The IL-6/sIL-6R complex is capable of activating cells via interaction with membrane-bound gp130. The molecular mass of IL-6/sIL-6R complex (~60 kDa) is about three-fold higher than that of IL-6 (~20 kDa). In this study, the IL-6/sIL-6R complex was made by incubating human recombinant IL-6 (3.3 μg/kg body weight) with an excess amount of human sIL-6R (33 μg/kg body weight) for 15 min at 37°C *in vitro*. For example, 9.9 μl of human recombinant IL-6 (100 ng/μl in ddH_2O) and 19.8 μl of human sIL-6R (500 ng/μl in PBS) were mixed for a rat weighting 300 g. Then we added normal saline to a final volume of 200 μl.

Male Wister rats weighing 270–325 g were anesthetized with sodium pentobarbital (50 mg/kg, i.p.) prior to surgery. Rats were randomly divided into five major groups: sham-operated rats ($n=4$), coronary occlusion and reperfusion rats administered IL-6/sIL-6R complex ($n=13$), a control vehicle ($n=13$), human recombinant IL-6 (3.3 μg/kg body weight, $n=11$), or human sIL-6R (33 μg/kg body weight, $n=11$). The volume of each drug is adjusted to 0.2 ml with a control vehicle, normal saline. The drugs were injected into the left ventricular cavity *in vivo* through the carotid cannula 15 min before coronary occlusion.

The animals were intubated and ventilated with a rodent respirator. A midline sternotomy was performed, and the heart was exposed. A reversible 4-0 silk slip knot was placed around the left coronary artery, approximately 5 mm distal from its origin, effectively occluding the vessel. Coronary occlusion was maintained for 30 min, at which time the slip knot was released, initiating reperfusion. Sham-operated control rats underwent the same surgical procedure except that the suture passed under the left coronary artery was not tied. We injected all the rats included sham-operated rats with 2 mg/kg of lidocaine through carotid catheter just after the coronary occlusion to prevent sustained ventricular tachycardia. After 3 h reperfusion, the left coronary artery was reoccluded briefly, and 1 ml phthalocyanine blue dye was injected into the left ventricular cavity *in vivo* and allowed to perfuse the nonischemic region of the heart, as previously reported.[34] Then, the heart was excised and divided into three regions: nonischemic, border, and ischemic.

In the experiments using tissue sections, we identified the border region as being at the edge of the blue-dye-stained region. This border region included both perfused myocardium and ischemic myocardium, because of interdigitation of intramyocardial coronary arteries. Therefore, in the extraction of genomic DNA, we identified the border region as the tissue mass which included an equal amount of the blue-dye-stained and nonblue-dye-stained region abutting the edge of the blue-dye-stained area, and whose total weight was approximately 100 mg.

The study was approved by the Keio University School of Medicine Care of Experimental Animals Committee.

Hemodynamic Evaluation

The right carotid artery was cannulated with a 22 G teflon catheter connected to a pressure transducer (Nihon Koden, Tokyo, Japan). By monitoring arterial blood pressure, the catheter was advanced into the

left ventricular cavity for evaluation of left ventricular pressure and also for injection of the drugs.

Infarct Sizing

After reperfusion, the left coronary artery was reoccluded briefly, and 1 ml phthalocyanine blue dye was injected into the left ventricular cavity *in vivo* and allowed to perfuse the nonischemic region of the heart. The entire heart was excised and sliced transversely into sections approximately 2 mm in thickness. The slices were photographed and then incubated in a 1% solution of tetrazolium chloride (TTC) for 10 min at 37°C to stain the viable myocardium brick red. The samples were fixed in 10% buffered formalin for 24 h and then photographed. The area at risk (regions not stained with phthalocyanine blue dye) and the infarcted area (regions not stained with TTC) were outlined on each photograph and measured using an image analyzer. Infarct size was expressed as a percentage of the infarcted area divided by the area at risk.

Agarose Gel Electrophoresis of DNA

Extracted genomic DNA was dissolved in TE buffer (10 mM Tris-HCl and 1 mM EDTA, pH 8.0) at 50°C overnight. The DNA solution was treated with RNase (100 μg/ml) for 1 h at 37°C.

In all, 12 μg of DNA was electrophoresed in 2% agarose gel in TAE buffer (40 mM Tris-HCl, 30 mM acetic acid, and 2 mM EDTA, pH 8.0) for 5 h at 50 V. After electrophoresis, the gel was stained in vistra green solution (Amersham, Buckinghamshire, UK), and the DNA was visualized using the Fluor imager (Molecular Dynamics Inc., CA, USA) as previously reported.[34] To confirm DNA ladder formation, the linear distribution of signal intensity for each lane was analyzed using the Image QuaNT software (Molecular Dynamics Inc.).

TdT-Mediated dUTP-Biotin Nick End Labeling (TUNEL)

Fragmented DNA was detected in myocardial sections using a modified end-labeling technique as previously reported.[34] Paraffin-embedded myocardial sections were mounted on glass slides. Nonischemic and ischemic area orientation was confirmed by phthalocyanine blue dye. The slides were incubated with 5 μg/ml of proteinase K for 15 min at room temperature (RT), and then the endogenous peroxidase was inactivated by immersing the sections in 2% H_2O_2. Deoxynucleotidyl transferase (0.3 U/ml) and biotinylated dUTP in TdT buffer (30 mM Tris-HCl, pH 7.2, 140 mM sodium cacodylate, 1 mM cobalt chloride) were added to cover the sections and the sections were incubated in a humid chamber at 37°C for 60 min. After washing, the sections were covered with streptavidin peroxidase for 15 min at RT, and then stained with 3,3′-diaminobenzidine tetrahydrochloride. The sections were counterstained with methyl-green. Positive control samples were prepared by incubating sections with DNase I prior to treatment with terminal transferase. Negative controls consisted of specimens in which deoxynucleotidyl transferase was omitted.

To determine the ratio of TUNEL-positive myocytes, the number of TUNEL-positive cardiomyocyte nuclei was divided by the total number of cardiomyocyte nuclei. Six representative microscopic fields were analyzed for each region.

Electron Microscope

The hearts were subjected to perfusion-fixation with Karnovsky's fixative before excision. Tissue samples from ischemic, border, and nonischemic regions were immersed in Karnovsky's fixative. Thin sections were mounted on grids; scanned and photographed.

Blood Analysis

The right femoral artery was cannulated with a 24 G teflon catheter to obtain blood samples. In all, 4 ml of arterial blood was drawn from the femoral artery immediately after 3 h reperfusion but before dye injection. In addition to blood counts, the plasma was separated and C-reactive protein (CRP) was quantified by Latex Agglutination-Turbidimetric Immunoassay, using LZ TEST 'EIKEN' CRP kit according to the manufacture's instruction (Eiken Chemical Co., Ltd., Tokyo, Japan).

Immunoprecipitation and Western Blot Analysis

Polyclonal antibodies to gp130 and monoclonal antibody to phosphotyrosine were obtained from Upstate Biotechnology (Lake Placid, NY, USA). Sham-operated rats were used for this experiment. Without the occlusion of the left coronary artery, LV tissues were harvested at 0, 5, 15, 30, and 60 min after the injection of IL-6/sIL-6R complex into LV cavity through the carotid catheter. LV tissues were homogenized in lysis buffer (150 mM NaCl, 0.02% sodium azide, 0.1% SDS, 100 μg/ml PMSF, 1 μg/ml aprotinin, 1% NP-40, 0.5% sodium deoxycholate, 50 mM NaF, 25 mM β-glycerophospate, and 1 mM Na_3VO_4 in 50 mM Tris-HCl, pH 8.0) and the 5 mg of lysates were precleared by incubation with protein G sepharose (Amersham Pharmacia Biotech, NJ, USA) for 1 h at 4°C. After centrifugation, the lysates were incubated with the monoclonal antibody to phosphotyrosine overnight at 4°C. Immunocomplexes were collected by incubating with 40 μl of protein G sepharose for 2 h. Immunoprecipitates were washed five times with TBS-T (0.1% tween-20 and 137 mM NaCl in 20 mM Tris-HCl, pH 7.6). The precipitated proteins were dissolved in sample buffer (10% glycerol, 2.3% SDS and 5% β-mercap-

toethanol in 62.5 mM Tris-HCl, pH 6.8) and heated at 95°C for 5 min. Proteins were separated by 7.5% sodium dodecyl sulfate-polyacrylamide gel electrophoresis (SDS-PAGE). Protein fractions were then electrophoretically transferred onto a polyvinylidene difluoride (PVDF) membrane. The membrane was blocked with 5% nonfat-dried milk in TBS-T. Then the membrane was incubated with rabbit polyclonal antibody to gp130 for 1 h at RT. The primary antibody was diluted 1:100 in blocking solution. After washing in TBS-T, it was incubated with horseradish peroxidase-conjugated swine anti-rabbit immunoglobulin diluted to 1:1000 in blocking solution. The antigen antibody–peroxidase complex was visualized using the ECL chemiluminescence detection kit (Amersham International, Buckinghamshire, UK).

Statistical Analysis

All values are expressed as the mean ± s.e.m. Statistical significance was determined using an ANOVA followed by the Bonferroni test. *P*-values less than 0.05 were considered statistically significant.

Results

Assessment of Infarct Size

Infarct size, or the percent infarct area, was evaluated as a percentage of infarct area to area at risk. Phthalocyanine blue dye and TTC staining were performed to estimate area at risk and infarct area, respectively (Figure 1a). The average area at risk was 45.9 ± 2.9% in the vehicle-treated group, 53.3 ± 3.1% in the IL-6/sIL-6R complex-treated group, 49.3 ± 3.8% in the IL-6-treated group, and 51.4 ± 2.5% in the sIL-6R-treated group, with no significant differences among the four groups (ANOVA). However, there were significant differences ($P = 0.0002$ by ANOVA) in the percentage of the infarct area relative to the area at risk (percent infarct area) among the IL-6/sIL-6R complex-treated (23.8 ± 1.8%), vehicle-treated (37.9 ± 3.7%), IL-6-treated (40.7 ± 1.0%), and sIL-6R-treated (37.5 ± 2.4%) groups (Figure 1b). The results of the Bonferroni test showed that only the IL-6/sIL-6R complex-treated group showed a significantly smaller ($P = 0.0004$) percent infarct area than the vehicle-treated group (three comparisons). The IL-6-treated and sIL-6R-treated groups showed no significant differences from the vehicle-treated group.

Heart Rate and Left Ventricular Pressure

ANOVA revealed no significant differences in the heart rate (HR), left ventricular systolic pressure, or left ventricular end diastolic pressure measured before coronary occlusion, after coronary occlusion, or after reperfusion among the vehicle-treated, IL-6/sIL-6R complex-treated, IL-6-treated, and sIL-6R-treated groups (Table 1). The reduction in the infarct size was not considered to be related to the HR or blood pressure, but to an antiapoptotic effect.

Cardiac Arrhythmias

Almost all arrhythmias occurred between 5 and 15 min after coronary occlusion. Some rats showed isolated premature ventricular contraction (PVC) just after the reperfusion but those arrhythmias were not severe. In this study, we injected all the rats included sham-operated rats with 2 mg/kg of lidocaine through carotid catheter just after the coronary occlusion to prevent sustained ventricular tachycardia (VT). Even after the injection of lidocaine, some rats still exhibited PVC or nonsustained VT between 5 and 15 min after coronary occlusion. However, they were transient and recovered without additional drugs. Although we did not observe the difference in arrhythmias among the vehicle-treated, IL-6/sIL-6R complex-treated, IL-6-treated, and sIL-6R-treated groups, we cannot exclude the possibility that lidocaine masked the difference in arrhythmias.

Blood Analysis

There were no significant differences in the white blood cell count or serum CRP level among the vehicle-treated, IL-6/sIL-6R complex-treated, IL-6-treated, and sIL-6R-treated groups (Table 2).

Agarose Gel Electrophoresis

Genomic DNA obtained from the ischemic and the border regions of the vehicle group showed typical DNA laddering with reduced high molecular weight genomic DNA. However, DNA from any region of the IL-6/sIL-6R complex group as well as from the nonischemic region of the vehicle group did not exhibit DNA fragmentation. DNA from nonischemic regions as well as specimens taken from the border region of the IL-6/sIL-6R complex group exhibited preservation of high molecular weight genomic DNA bands (Figure 2). Similar to the vehicle group, DNA from the ischemic and the border regions of the IL-6 or sIL-6R group showed typical DNA laddering with reduced high molecular weight genomic DNA (Figure 3). Thus, specimens taken from only the IL-6/sIL-6R complex group exhibited inhibition of cardiomyocyte apoptosis following reperfusion.

In Situ DNA Fragmentation by TUNEL Staining

To visualize apoptosis *in situ*, the TUNEL method was employed to detect apoptotic nuclei in myocardial cells. In the nonischemic regions, positively stained nuclei were rarely detected in the rat hearts.

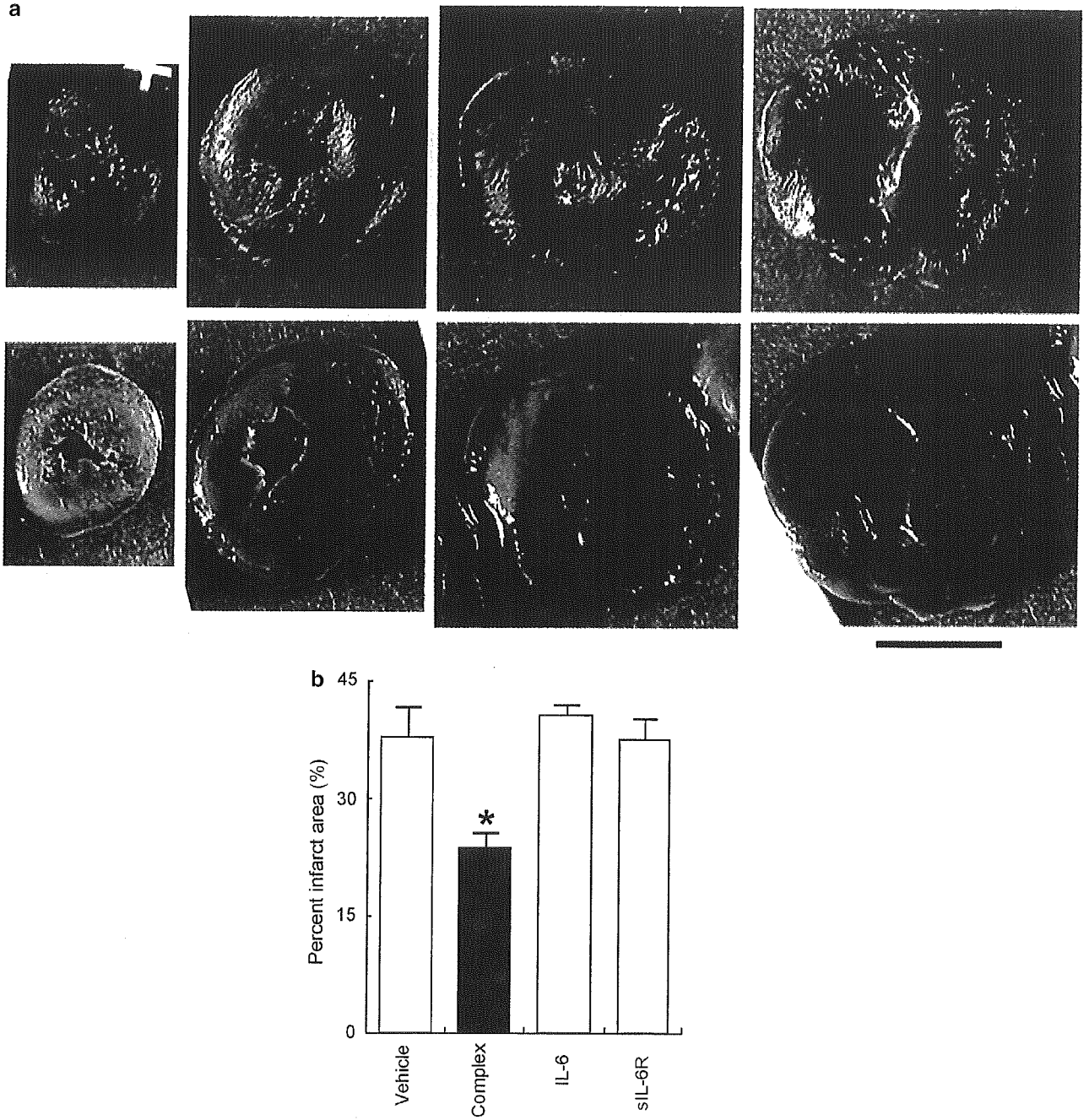

Figure 1 Assessment of infarct size. (**a**) Photos of rat hearts showing phthalocyanine blue dye and tetrazolium chloride (TTC) staining. The heart was sliced transversely into sections approximately 2 mm in thickness. The area at risk was defined as regions not stained with phthalocyanine blue dye, shown in the upper panels, and the infarct area was defined as regions not stained with TTC (white area), shown in the lower panels. Each pair of upper and lower panels represents the same slice. The infarct size, or the percent infarct area, was evaluated as a percentage of the infarct area relative to the area at risk. Bar represents 5 mm. (**b**) Bar graph representing the percentage of the infarct area relative to the area at risk in rat hearts subjected to 30 min ischemia and 3 h reperfusion after the administration of the control vehicle, IL-6, sIL-6R, or the IL-6/soluble IL-6R complex. The drugs were injected *in vivo* into the LV cavity through a carotid cannula 15 min before coronary occlusion. The percentage of infarct area relative to the area at risk was significantly smaller in the IL-6/sIL-6R complex-treated group ($23.8 \pm 1.8\%$, $n=7$) than in the vehicle-treated ($37.9 \pm 3.7\%$, $n=7$), IL-6-treated ($40.7 \pm 1.0\%$, $n=7$), and sIL-6R-treated ($37.5 \pm 2.4\%$, $n=7$) groups. $^*P<0.05$ *vs* vehicle-, IL-6-, and sIL-6R-treated groups. The error bar represents the s.e.m.

In the ischemic or border regions of the vehicle hearts, numerous TUNEL-positive nuclei were observed. However, in the ischemic and border regions of the IL-6/sIL-6R complex-treated hearts, only scattered positive nuclei were observed and there were considerably less positive nuclei compared with the vehicle-treated hearts (Figure 4). Similar to the vehicle hearts, numerous TUNEL-positive nuclei were observed in the ischemic or border regions of the IL-6-treated or sIL-6R-treated hearts (Figure 5).

Table 1 Heart rate and left ventricular pressure

	Vehicle	*Complex*	*IL-6*	*sIL-6R*
Heart rate (bpm)				
Baseline	395±20	398±17	361±8	335±25
occ 30	312±19	330±11	310±13	291±24
rep 30	310±22	345±17	325±18	313±28
rep 180	288±18	345±12	294±12	289±18
LVSP (mmHg)				
Baseline	107±6	109±6	126±4	116±3
occ 30	94±3	104±4	99±4	89±8
rep 30	96±5	115±3	104±5	105±8
rep 180	113±4	125±5	107±5	106±7
LVEDP (mmHg)				
Baseline	6.7±1.1	5.9±1.1	4.3±0.7	6.4±0.5
occ 30	5.6±0.7	7.6±0.6	8.4±1.0	9.6±1.1
rep 30	5.6±1.5	8.6±0.7	10.2±1.1	7.4±1.1
rep 180	5.9±0.6	7.9±0.8	5.4±0.2	6.6±0.6

Complex = IL-6/sIL-6R complex; IL-6 = interleukin-6; LVEDP = left ventricular end diastolic pressure; LVSP = left ventricular systolic pressure; occ = occlusion; rep = reperfusion; sIL-6R = soluble interleukin-6 receptor.

Table 2 Blood analysis

	Vehicle	*Complex*	*IL-6*	*sIL-6R*
WBC (/μl)	8600±1120	7644±566	6560±733	6250±517
CRP (mg/dl)	0.1±0.02	0.1±0.02	0.1±0.02	0.1±0.02

Complex = IL-6/sIL-6R complex; CRP = C-reactive protein; IL-6 = interleukin-6; sIL-6R = soluble interleukin-6 receptor; WBC = white blood cell count.

Quantitatively, the ratio of TUNEL-positive myocytes in the ischemic (I) and border (B) regions was significantly smaller in the IL-6/sIL-6R complex-treated group (I: 4.8±0.6%, B: 3.9±0.7%) than that in the vehicle-treated (I: 14.1±0.7%, B: 13.9±0.9%), IL-6-treated (I: 13.1±0.7%, B: 13.2±0.8%), and sIL-6R-treated (I: 14.9±1.0%, B: 12.9±1.1%) groups ($P<0.0001$ by ANOVA, $P<0.0001$ by Bonferroni test when comparing with the vehicle group in the same region, three comparisons in each region) (Figure 6). No significant differences were observed among the vehicle-treated, IL-6-treated, and sIL-6R-treated groups.

Electron Microscope Findings

To confirm cardiomyocyte apoptosis, we analyzed the vehicle-treated border and ischemic tissue sections by electron microscope. The ultrastructural features of apoptotic cells are known to be shrunk cells displaying segregation of chromatin into discrete clumps abutting the nuclear membrane, whereas cytoplasmic organelles most often kept a normal appearance.[35] In the vehicle-treated border and ischemic sections, apoptotic myocytes presented with complete nuclear chromatin condensation along the nuclear membrane (Figure 7). Consistent with previous studies on myocardial ischemia/reperfusion,[26,27] we were not able to detect definite apoptotic bodies of cardiomyocyte origin in these sections.

Activation of gp130 by IL-6/sIL-6 Receptor Complex

To confirm the gp130 pathway is activated by the injection of IL-6/sIL-6R complex, we examined the tyrosine phosphorylation of gp130 in rat hearts. As shown in Figure 8, basal level of tyrosine phosphorylation of gp130 was very little but significant tyrosine phosphorylation of gp130 was observed in rat hearts after the infection of IL-6/sIL-6R complex. Intense phosphorylation of gp130 was observed between 5 and 15 min after injection. These results indicate that the IL-6/sIL-6R complex activates gp130 pathway.

Assessment of Left Ventricular Function by LV d*P*/d*t*

Having demonstrated that our IL-6/soluble IL-6R complex reduces infarct size through inhibiting myocardial apoptosis, we compared LV function using LV d*P*/d*t* between vehicle-treated rats and IL-6/sIL-6R complex treated rats. Since LV d*P*/d*t* is very sensitive to inotrophic changes, it is considered to be a good marker which reflects LV function.[36–38] As shown in Table 3, trends towards higher positive d*P*/d*t* and negative d*P*/d*t* were observed at 30 min after occlusion and at 30 min after reperfusion in IL-6/sIL-6 complex group; however, these differences did not reach statistical significance.

Discussion

In this study, we have shown that administration of IL-6/sIL-6R complex inhibits apoptosis in the reperfused myocardium. Furthermore, the above complex was also able to reduce infarct size. IL-6/sIL-6R complex has been reported to have various functions in the central nervous system, the hematopoietic system, and other tissues;[1–6] however, the effect of the complex in myocardial infarction has not been directly assessed so far. This is the first report of the possible therapeutic effects of IL-6/sIL-6R complex in reperfused myocardial infarction; our results suggest the possible use of this complex in the clinical treatment of reperfused myocardial infarction as well as other cardiac diseases involving apoptosis such as myocarditis and heart failure.[39,40]

IL-6/sIL-6R complex induces the homodimerization of gp130. Homodimerization of the two gp130 molecules causes phosphorylation of gp130 and the transcription factors STAT1 and STAT3 by Janus-Kinases (JAK1, JAK2, TYK2) and then acti-

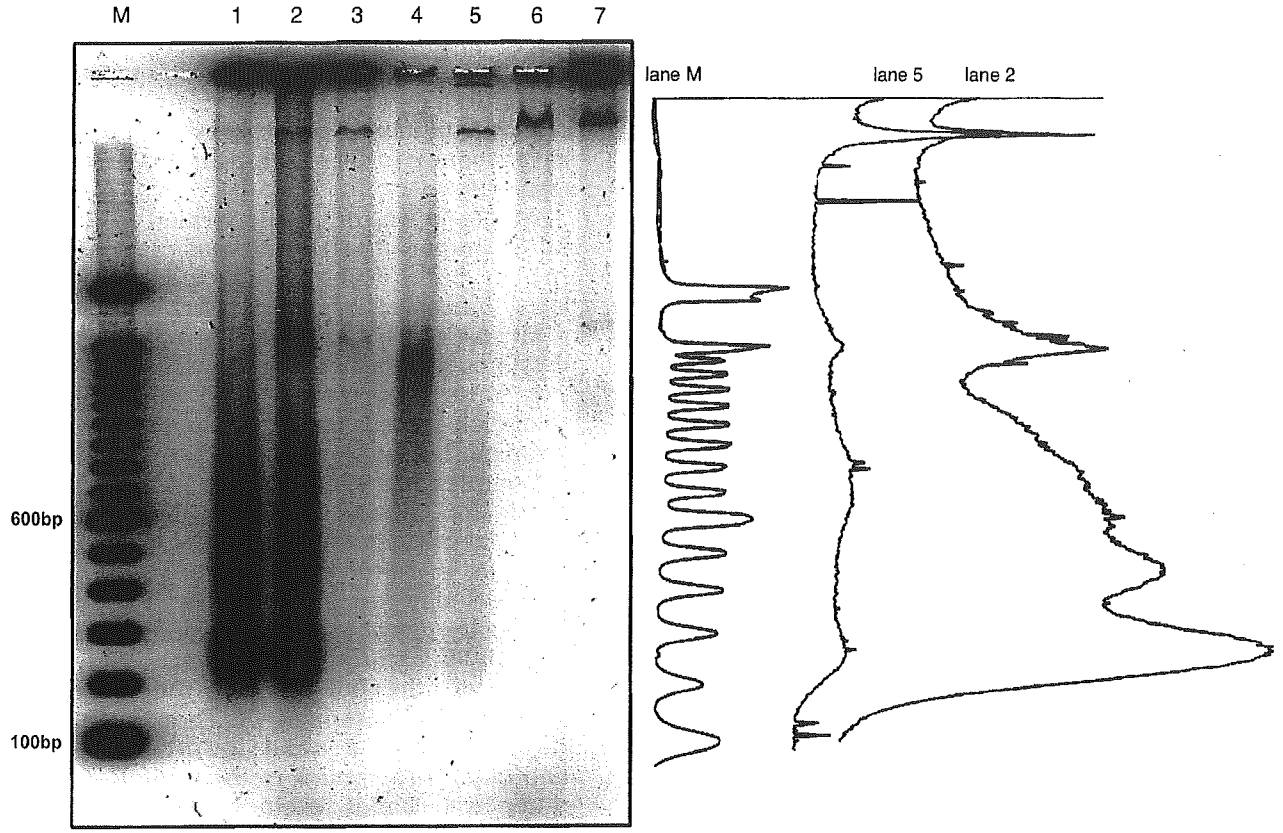

Figure 2 DNA ladder formation in rat heart administered either a control vehicle or IL-6/sIL-6R complex. Genomic DNA was extracted from rat myocardium and electrophoresed in 2% agarose gel. Lanes 1–3 represent genomic DNA extracted from a heart exposed to 30 min ischemia and 3 h reperfusion and administered a control vehicle. Lanes 4–6 represent genomic DNA from a heart exposed to 30 min ischemia and 3 h reperfusion and administered the IL-6/sIL-6R complex (lanes 1 and 4: ischemic myocardium; lanes 2 and 5: border region myocardium; lanes 3 and 6: nonischemic myocardium). Genomic DNA from the ischemic and border regions (lanes 1 and 2) exhibited typical DNA laddering in the 200–600 bp range; however, genomic DNA from the nonischemic region (lane 3) exhibited preservation of high molecular weight DNA and did not exhibit DNA ladder formation typical of DNA fragmentation. In the IL-6/sIL-6R complex treated rat heart, the ischemic myocardium exhibited a smear pattern typical of degradated genomic DNA and did not exhibit DNA ladder formation. Genomic DNA from the border and nonischemic regions did not exhibit DNA ladder formation but did exhibit preservation of high molecular weight DNA. Lane 7 represented genomic DNA from a sham-operated heart and exhibited only the intact high molecular weight DNA band. M represents a 100 bp DNA ladder marker. The graph on the right represents the linear distribution of signal intensity of the agarose gel DNA electrophoresis for lanes M, 5, and 2 (M: marker lane; 5 and 2: lanes representing DNA from the border regions of the IL-6/sIL-6R complex treated and control vehicle-administered hearts, respectively). This distribution pattern confirms that typical DNA laddering can be detected in lane 2 but not in lane 5. DNA from individual hearts were used. The experiment shown is representative of three experiments.

vates cellular signal processes.[6,12,41–44] Our study indicated that administration of IL-6/sIL-6R complex, but not of IL-6 or sIL-6R alone, inhibited cardiomyocyte apoptosis in reperfused acute myocardial infarction. In this relation, it is of interest that coadministration of IL-6 and sIL-6R, but not IL-6 or sIL-6R alone attenuated motor dysfunction and neuropathological changes in wobbler mouse motor neuron disease.[45] Transgenic mice overexpressing both IL-6 and IL-6R present with hypertrophy of ventricular myocardium with advancing age; the myocardium in these animals has been shown to express gp130.[46] However, transgenic mice overexpressing IL-6 or IL-6R alone did not present with detectable myocardial abnormalities. The present study also showed that administration of IL-6 or sIL-6R alone had no effects on cardiomyocytes. In IL-6 signaling, the activation of STAT3 was shown to be linked with antiapoptotic signals through the induction of bcl-2.[13] Possible mechanism in our results is that exogenous IL-6/sIL-6R complex acts directly on cardiomyocytes by activating membrane-anchored gp130 and inhibits cardiomyocyte apoptosis. Another possibility is that the above complex may act on other cell types (eg, leukocytes) and reduce reperfusion injury through altering the myocardial environment. Since we showed that IL-6/sIL-6R complex induced tyrosine phosphorylation of gp130 within 5 min, we speculate the former mechanism is a more reasonable explanation for our results. Other studies also showed that IL-6/sIL-6R complex as well as ciliary neurotrophic factor and leukemia inhibitory factor—members of the IL-6 family—reached to the cell surface of target organs

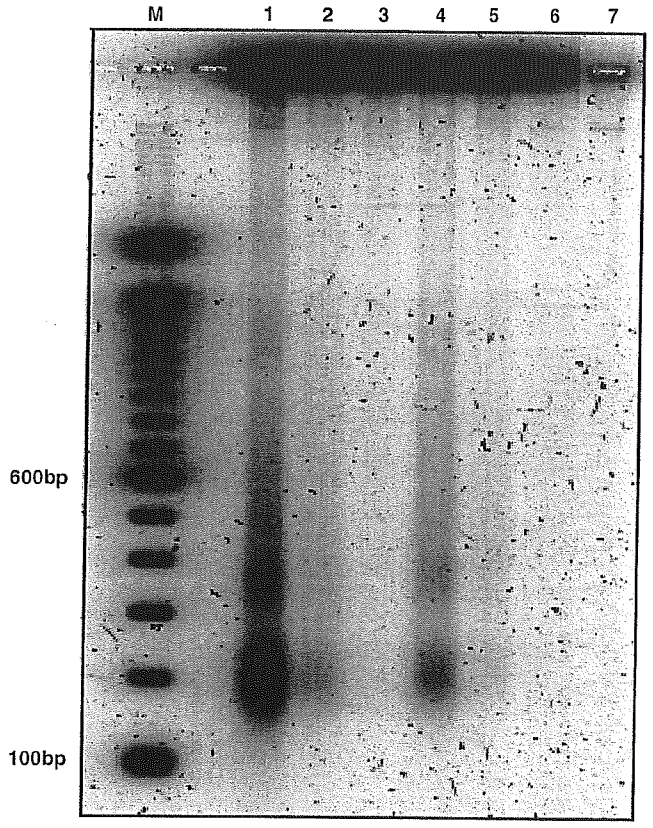

Figure 3 DNA ladder formation in rat heart administered either IL-6 or sIL-6R. Lanes 1–3 represent genomic DNA extracted from a heart exposed to 30 min ischemia and 3 h reperfusion and administered IL-6. Lanes 4–6 represent genomic DNA from a heart exposed to 30 min ischemia and 3 h reperfusion and administered sIL-6R (lanes 1 and 4: ischemic myocardium; lanes 2 and 5: border region myocardium; lanes 3 and 6: nonischemic myocardium). Genomic DNA from the ischemic and border regions (lanes 1, 2, 4, and 5) exhibited typical DNA laddering in the 200–600 bp range; however, genomic DNA from the nonischemic region (lanes 3 and 6) exhibited preservation of high molecular weight DNA and did not exhibit DNA ladder formation typical of DNA fragmentation. Lane 7 represented genomic DNA from a sham-operated heart and exhibited only the intact high molecular weight DNA band. M represents a 100 bp DNA ladder marker. DNA from individual hearts were used. The experiment shown is representative of three experiments.

and had therapeutic effects after systemic administration.[45,47,48]

Our results demonstrated that myocardial apoptosis was inhibited by IL-6/sIL-6R complex in the border region as well as the nonischemic region. The characteristics of the border region are considered to differ from those of normal myocardium. Myocardial infarction induces regional abnormalities (asynergy) in the wall motion of the heart. The infarcted region presents with akinesis; subsequently, the border region adjacent to the ischemic region is subjected to mechanical stretching. This mechanical stretching can trigger certain signals associated with apoptosis.[49] In addition, an increased workload in the border region requires an increase in oxidative metabolism for energy production; the resulting oxidative stress may activate certain signaling pathways and promote apoptosis.[50,51]

Although our results provide provocative and stimulating possibilities in treatment and suggest new orientations in clinical research topics, several issues require further investigations prior to clinical application.

Apoptosis was originally termed to define essential programmed cell death and plays an important role in both development and maintenance of tissue homeostasis.[52–54] In other words, this form of altruistic cell death can be considered to be a physiologically fundamental method of ridding the body of unnecessary cells and can be considered a beneficial process in response to damage to the organism. Indeed, we have shown that the IL-6/sIL-6R complex can reduce infarct size and attenuate reperfusion injury; however, it remains to be established whether rescue of these dying myocytes leads to a better clinical prognosis. Inhibiting apoptosis may possibly leave the 'rescued' myocytes electrically unstable and may lead to fatal arrhythmias. In this study, we injected all the rats with 2 mg/kg of lidocaine just after the coronary occlusion to prevent sustained VT. Then, even though we did not observe a trend towards more frequent ventricular arrhythmias in the IL-6/sIL-6R complex group, we cannot exclude the possibility that lidocaine masked the difference in arrhythmias. Further investigations are required to correctly address this problem prior to actual clinical application.

It can be argued that in these ischemia/reperfusion models, including our own, cell death occurs via two major pathways; that is, apoptosis and necrosis. While these two modes of death are mutually exclusive, they may very well coexist. Shimizu *et al*[55] showed that Bcl-2 and Bcl-xL, both antiapoptotic proteins, protected mitochondria against loss of function, not only in apoptosis, but also in the process of necrosis. It has also been reported that both apoptosis and necrosis share common mediators and pathways leading to the final stages of cell death.[56] To take discussion of this complicated issue further, although DNA degradation is caused by both necrosis and apoptosis, the pattern of degradation between the two processes is different. While necrosis degrades genomic DNA in a smear pattern, apoptosis degrades genomic DNA in the ladder form. In this study, the IL-6/sIL-6R complex was shown to inhibit DNA ladder formation. We thus suggest that the IL-6/sIL-6R complex contributes mainly to inhibition of apoptosis rather than to that of necrosis; however, it is difficult to differentiate between these two forms of cell death based solely on the experimental protocols used in this study. Further experiments are necessary to clarify this complicated issue.

IL-6 induces expression of the intercellular adhesion molecule-1 (ICAM-1), a mediator of neutro-

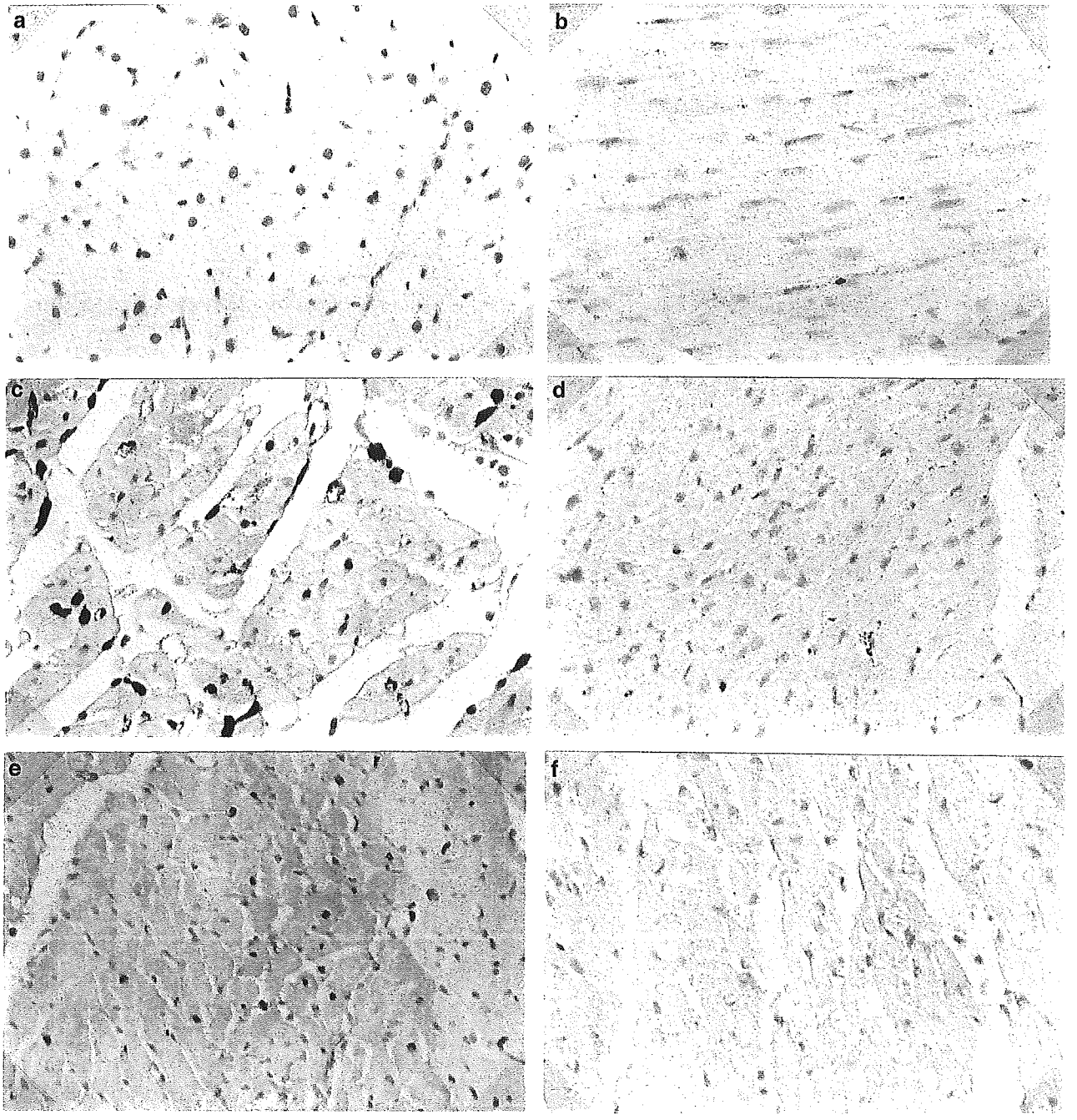

Figure 4 TUNEL staining of rat heart administered either a control vehicle or IL-6/sIL-6R complex. Tissue specimens were treated with DNA polymerase I and biotinylated dUTP, and visualized with streptavidin peroxidase and diaminobenzidine-hydrogen peroxide. Specimens were counterstained with methyl-green. Original magnification, × 200. (**a**) Positive control: cardiac tissue specimen exposed to DNase I prior to nick end labeling. The nuclei are represented by the positive brown staining. (**b**) Nonischemic myocardium exposed to 30 min of ischemia followed by 3 h of reperfusion administered a control vehicle. The nuclei are stained light green by the counterstain. (**c**) and (**d**) Specimens from the border region between nonischemic and ischemic myocardium exposed to 30 min of ischemia followed by 3 h of reperfusion. The blue coloring indicates blood flow from phthalocyanine blue dye. (**c**) Represents a cardiac specimen from a rat administered a control vehicle, and (**d**) from a rat administered the IL-6/sIL-6R complex. In (**c**), numerous positive brown reaction products can be observed in the nuclei of apoptotic cells. In (**d**), the number of apoptotic nuclei is markedly reduced. (**e**) and (**f**) Specimens from ischemic regions exposed to 30 min of ischemia followed by 3 h of reperfusion. Ischemia was confirmed by the absence of blue dye. (**e**) Represents a specimen from a rat administered a control vehicle, and (**f**) from a rat administered the above complex. Similar to the findings in the border region, the number of apoptotic nuclei is markedly reduced following administration of the complex.

phil-induced injury, and promotes inflammation.[57–60] In the myocardial ischemia–reperfusion model, Kukielka *et al*[59] showed that IL-6 played an important role in the induction of ICAM-1 in the ischemic regions. Regarding the clinical study also, Ohtsuka *et al*[61] clearly showed that serum levels of

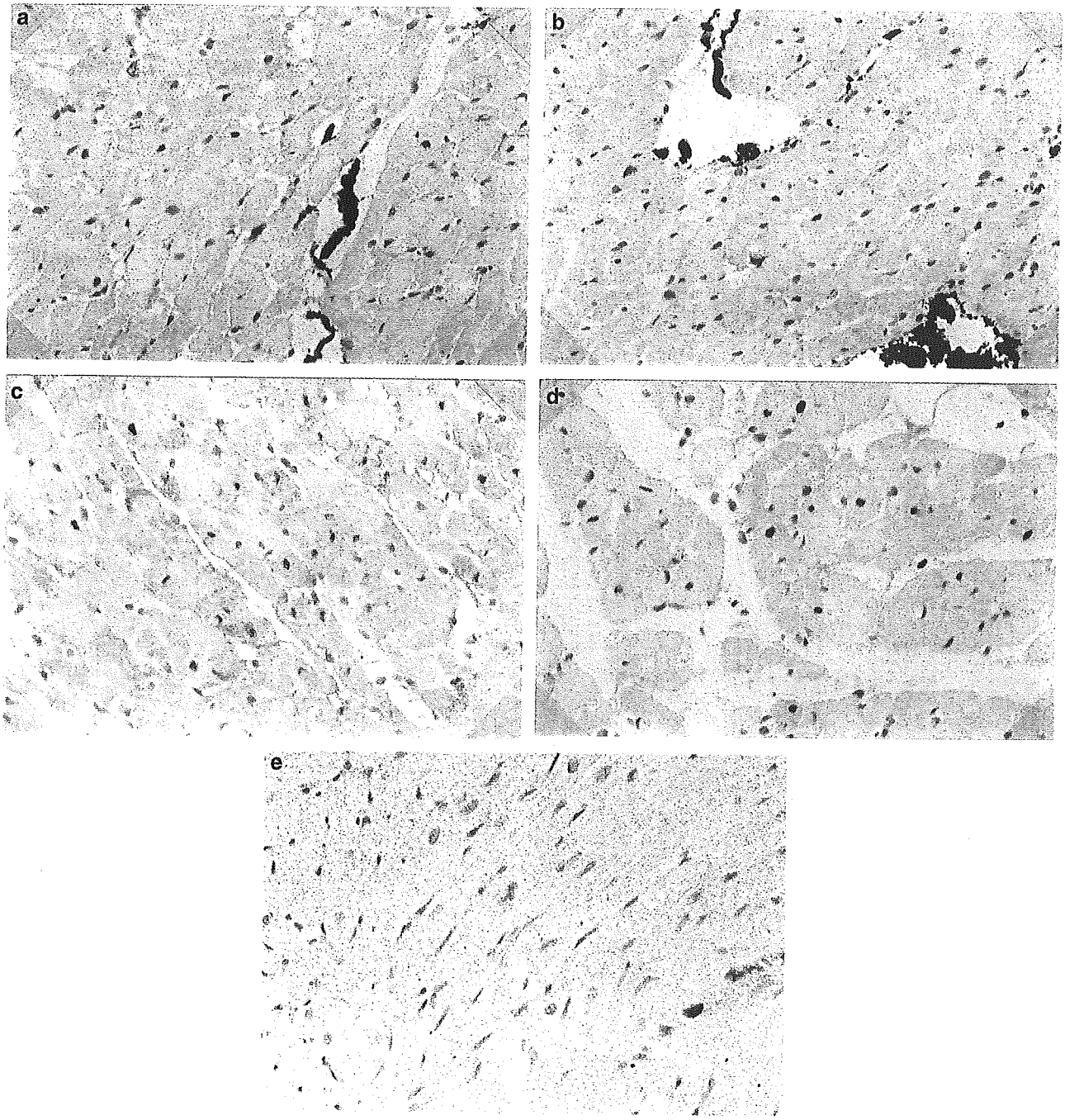

Figure 5 TUNEL staining of rat heart administered either IL-6 or sIL-6R. (**a**) and (**b**) Specimens from the border region between nonischemic and ischemic myocardium exposed to 30 min of ischemia followed by 3 h of reperfusion. The blue coloring indicates blood flow from phthalocyanine blue dye. (**a**) Represents a cardiac specimen from a rat administered IL-6, and (**b**) from a rat administered sIL-6R. (**c**) and (**d**) Specimens from ischemic regions exposed to 30 min of ischemia followed by 3 h of reperfusion. Ischemia was confirmed by the absence of blue dye. (**c**) Represents a specimen from a rat administered IL-6, and (**d**) from a rat administered IL-6R. In (**a**)–(**d**), numerous TUNEL-positive nuclei can be observed. (**e**) Represents a specimen obtained from a sham operation. The nuclei are stained light green by the counterstain. Original magnification, ×200.

IL-6 correlated well negatively with the change in the reduction of LV end-diastolic volume index 6 months after onset of myocardial infarction. They concluded that circulating IL-6 at the acute phase is a powerful independent predictor of LV remodeling after reperfused myocardial infarction.[61] Therefore, we have to consider potential adverse effects of IL-6 and potential effects of IL-6 and IL-6/sIL-6R complex on ventricular remodeling. The balance between the proinflammatory adverse effect and antiapoptotic cytoprotective effect of IL-6 and the IL-6/sIL-6R complex is important. In this study, there were no significant differences in the white blood cell count or serum CRP level among the

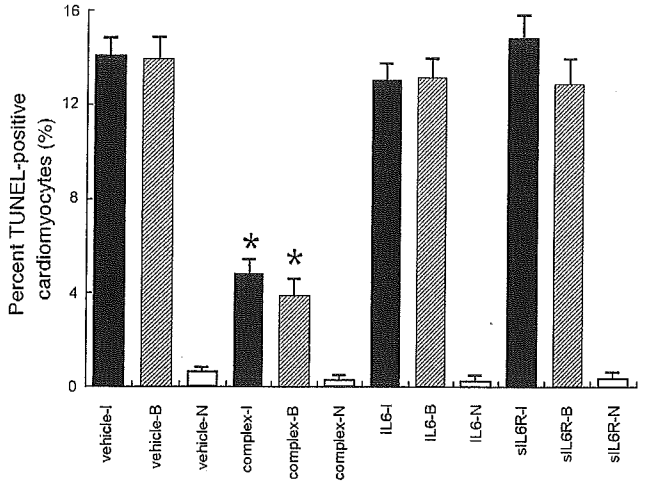

Figure 6 Bar graph representing the ratio of TUNEL-positive myocytes in rat heart specimens. The number of TUNEL-positive cardiomyocyte nuclei was divided by the total number of cardiomyocyte nuclei to determine the ratio of TUNEL-positive myocytes. In ischemic (I: solid bars) and border (B: hatched bars) regions, the ratio of TUNEL-positive myocytes in the IL-6/sIL-6R complex group was significantly smaller than that in the vehicle, the IL-6, or the sIL-6R groups. In the nonischemic (N: open bars) regions, TUNEL-positive myocytes were rarely detected in the rat hearts. Six representative microscopic fields were analyzed for each region. $^*P<0.05$ *vs* vehicle, IL-6, or sIL-6R in each region. The error bar represents the s.e.m.

vehicle-treated, IL-6/sIL-6R complex-treated, IL-6-treated, and sIL-6R-treated groups. However, we used an acute model, and it is possible that injection of the IL-6 or IL-6/sIL-6R complex is associated with upregulation of the inflammatory response during the chronic phase. Although the antiapoptotic cytoprotective effect of the complex was thought to be stronger than its proinflammatory effect in our acute model, the balance may be changed in a chronic model. More data will be needed before the

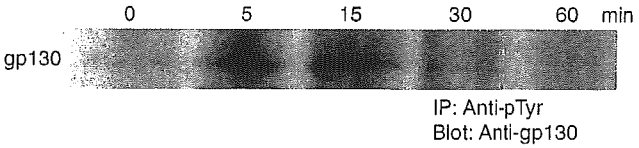

Figure 8 Time course of gp130 phosphorylation after the injection of IL-6/sIL-6R complex. Tissue samples obtained from left ventricle were examined at various times after injection of IL-6/sIL-6R complex into LV cavity. Equal amount of proteins from left ventricle of rat hearts obtained 0, 5, 15, 30, and 60 min after injection of IL-6/sIL-6R complex were lysed with lysis buffer, immunoprecipitated with antiphosphotyrosine antibody, separated by 7.5% SDS-PAGE, and transferred onto a polyvinylidene difluoride (PVDF) membrane. The blot was probed with anti-gp130 antibody. The experiment shown is representative of three experiments.

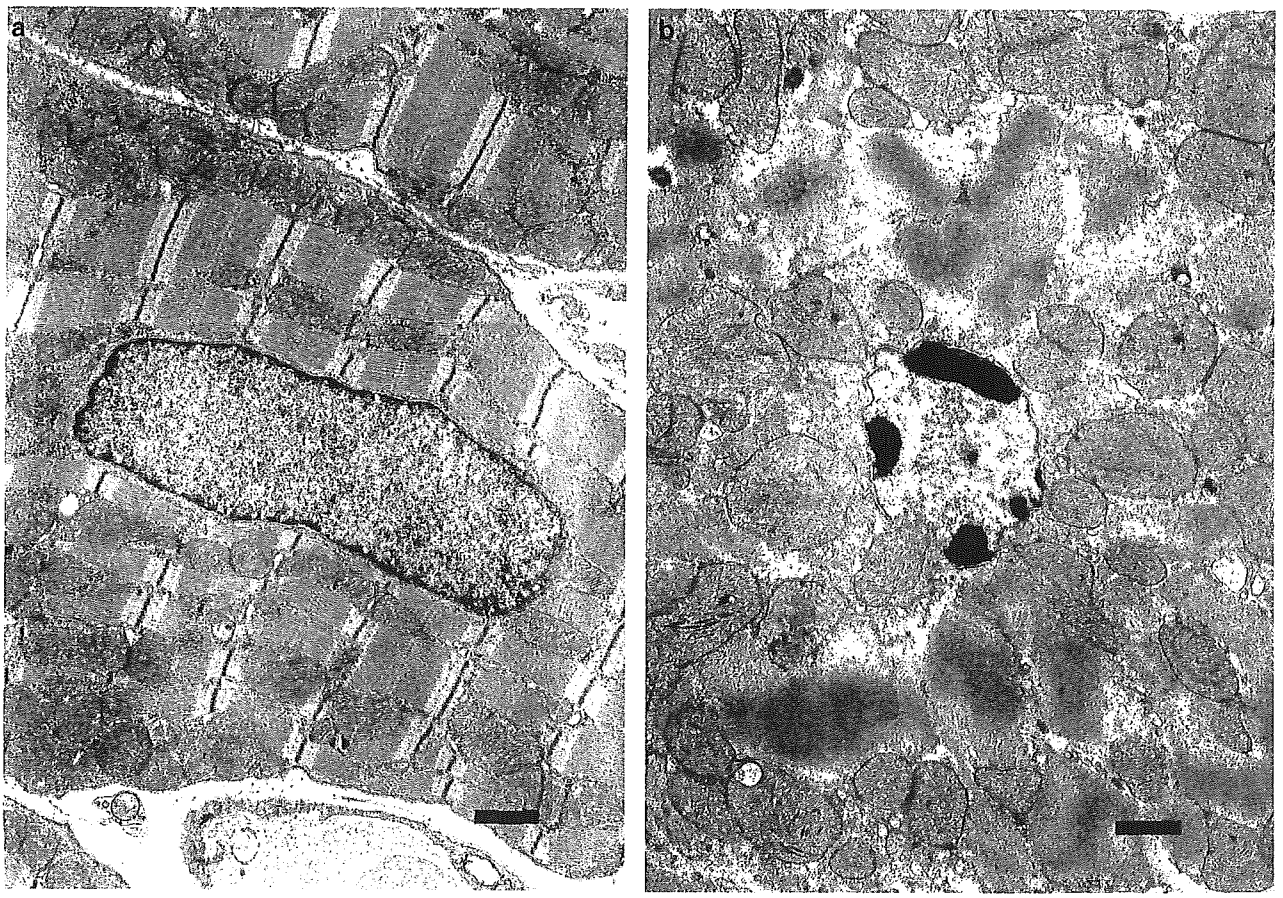

Figure 7 Electron micrographs of cardiomyocytes. (**a**) Cardiomyocyte specimen taken from a sham operation. (**b**) Cardiomyocyte specimen of the border region exposed to 30 min ischemia and 3 h reperfusion administered a control vehicle. Apoptotic myocytes present with chromatin condensation along the nuclear membrane. Bar represents 1 μm.

Table 3 Left ventricular d*P*/d*t* (positive and negative)

	LV dP/dt (positive/negative), mmHg/s	
	Vehicle	*IL-6/sIL-6R complex*
Baseline	+4667±422/−2850±275	+4620±543/−2820±260
occ 30	+3567±340/−2292±187	+4650±650/−3225±439
rep 30	+3714±264/−2571±277	+4940±542/−3280±256
rep 180	+4429±468/−3214±343	+4130±356/−3180±433

IL-6 = interleukin-6; sIL-6R = soluble interleukin-6 receptor; occ = occlusion; rep = reperfusion.

clinical implications of the actions of this complex become clearer.

In our models, the effects of the drugs were produced by a systemic injection, rather than a coronary injection. Hajjar *et al*[62] occluded the aorta and pulmonary artery to insure that the coronary arteries were perfused for gene delivery studies *in vivo*. If the drugs in the present study had been delivered to the coronaries with the large vessel occlusions, the effect might have been larger than the result we obtained. It is also very important how long the drug can keep its effects. Peters *et al*[63] examined how long the exogenous IL-6 or IL-6/sIL-6R complex lasted. They injected mice intraperitoneally with either 40 μg of IL-6 or 4 μg of IL-6/sIL-6R complex per mouse and investigated the acute phase response gene expression in the livers of those mice. Their results showed that the effect of 40 μg of IL-6 lasted 24 h and the effect of 4 μg of IL-6/sIL-6R complex lasted 72 h. The gene expression in mice received IL-6/sIL-6R complex was much stronger than that in mice received IL-6. They concluded that the IL-6/sIL-6R complex is active markedly long.[63] Whether cardiomyocytes express the IL-6 receptor is controversial. Youker *et al*[20] showed that IL-6 activated the IL-6 signal pathway in cardiomyocytes. In target cells expressing membrane-bound IL-6 receptors, the function of IL-6 is further augmented by the addition of sIL-6Rs.[17,18] Although IL-6 alone had no effect on cardiomyocyte apoptosis in our models, IL-6 alone might have been effective if large vessel occlusions had been used. Technically, the administration of the IL-6/sIL-6R complex can be clinically implemented in humans by selectively injecting the IL-6/sIL-6R complex into the target coronary artery during primary angioplasty or intracoronary thrombolysis.

In conclusion, the present study demonstrates for the first time that the IL-6/sIL-6 receptor complex is effective in ameliorating reperfusion injury in acute myocardial infarction. This effect may be more dramatic in humans; this is because only systemic administration was possible in our experimental rat models whereas more selective administration would be possible in humans. Thus our results hint at possible novel therapies for acute myocardial infarction.

Acknowledgements

We greatly appreciate Dr Tadamitsu Kishimoto (Osaka University) for providing us with human soluble IL-6 receptor. We are also grateful to Dr Atsushi Suzuki for his criticism and discussion. In addition, we are grateful to Mr Naomichi Yagi, Ms Yuko Hashimoto, Mr Satoshi Kusakari and Mr Hitoshi Abe for their technical assistance.

Conflict of interest

There is no conflict of interest and financial disclosure. No financial support was received.

References

1 Tamura T, Udagawa N, Takahashi N, *et al.* Soluble interleukin-6 receptor triggers osteoclast formation by interleukin 6. Proc Natl Acad Sci USA 1993;90: 11924–11928.
2 Mihara M, Moriya Y, Ohsugi Y. IL-6-soluble IL-6 receptor complex inhibits the proliferation of dermal fibroblasts. Int J Immunopharmacol 1996;18:89–94.
3 Gaillard JP, Liautard J, Klein B, *et al.* Major role of the soluble interleukin-6/interleukin-6 receptor complex for the proliferation of interleukin-6-dependent human myeloma cell lines. Eur J Immunol 1997;27:3332–3340.
4 Kordula T, Rydel RE, Brigham EF, *et al.* Oncostatin M and the interleukin-6 and soluble interleukin-6 receptor complex regulate alpha1-antichymotrypsin expression in human cortical astrocytes. J Biol Chem 1998; 273:4112–4118.
5 Marz P, Herget T, Lang E, *et al.* Activation of gp130 by IL-6/soluble IL-6 receptor induces neuronal differentiation. Eur J Neurosci 1997;9:2765–2773.
6 Kallen KJ. The role of transsignalling via the agonistic soluble IL-6 receptor in human diseases. Biochim Biophys Acta 2002;1592:323–343.
7 Rose-John S, Heinrich PC. Soluble receptors for cytokines and growth factors: generation and biological function. Biochem J 1994;300(Part 2):281–290.
8 Jones SA, Horiuchi S, Topley N, *et al.* The soluble interleukin 6 receptor: mechanisms of production and implications in disease. FASEB J 2001;15:43–58.
9 Saito M, Yoshida K, Hibi M, *et al.* Molecular cloning of a murine IL-6 receptor-associated signal transducer, gp130, and its regulated expression *in vivo*. J Immunol 1992;148:4066–4071.
10 Schindler R, Mancilla J, Endres S, *et al.* Correlations and interactions in the production of interleukin-6 (IL-6), IL-1, and tumor necrosis factor (TNF) in human blood mononuclear cells: IL-6 suppresses IL-1 and TNF. Blood 1990;75:40–47.
11 Tilg H, Trehu E, Atkins MB, *et al.* Interleukin-6 (IL-6) as an anti-inflammatory cytokine: induction of circulating IL-1 receptor antagonist and soluble tumor necrosis factor receptor p55. Blood 1994;83:113–118.
12 Heinrich PC, Behrmann I, Muller-Newen G, *et al.* Interleukin-6-type cytokine signalling through the gp130/Jak/STAT pathway. Biochem J 1998;334(Part 2): 297–314.

13 Fukada T, Hibi M, Yamanaka Y, *et al.* Two signals are necessary for cell proliferation induced by a cytokine receptor gp130: involvement of STAT3 in anti-apoptosis. Immunity 1996;5:449–460.
14 Lichtenstein A, Tu Y, Fady C, *et al.* Interleukin-6 inhibits apoptosis of malignant plasma cells. Cell Immunol 1995;162:248–255.
15 Hitzler JK, Martinez-Valdez H, Bergsagel DB, *et al.* Role of interleukin-6 in the proliferation of human multiple myeloma cell lines OCI-My 1 to 7 established from patients with advanced stage of the disease. Blood 1991;78:1996–2004.
16 Kawano M, Hirano T, Matsuda T, *et al.* Autocrine generation and requirement of BSF-2/IL-6 for human multiple myelomas. Nature 1988;332:83–85.
17 Honda M, Yamamoto S, Cheng M, *et al.* Human soluble IL-6 receptor: its detection and enhanced release by HIV infection. J Immunol 1992;148:2175–2180.
18 Taga T, Hibi M, Hirata Y, *et al.* Interleukin-6 triggers the association of its receptor with a possible signal transducer, gp130. Cell 1989;58:573–581.
19 Kunisada K, Tone E, Fujio Y, *et al.* Activation of gp130 transduces hypertrophic signals via STAT3 in cardiac myocytes. Circulation 1998;98:346–352.
20 Youker K, Smith CW, Anderson DC, *et al.* Neutrophil adherence to isolated adult cardiac myocytes. Induction by cardiac lymph collected during ischemia and reperfusion. J Clin Invest 1992;89:602–609.
21 Chandrasekar B, Mitchell DH, Colston JT, *et al.* Regulation of CCAAT/Enhancer binding protein, interleukin-6, interleukin-6 receptor, and gp130 expression during myocardial ischemia/reperfusion. Circulation 1999;99:427–433.
22 Fliss H, Gattinger D. Apoptosis in ischemic and reperfused rat myocardium. Circ Res 1996;79: 949–956.
23 Ryan TJ, Antman EM, Brooks NH, *et al.* 1999 update: ACC/AHA Guidelines for the Management of Patients With Acute Myocardial Infarction: Executive Summary and Recommendations: A report of the American College of Cardiology/American Heart Association Task Force on Practice Guidelines (Committee on Management of Acute Myocardial Infarction). Circulation 1999;100:1016–1030.
24 Braunwald E, Kloner RA. Myocardial reperfusion: a double-edged sword? J Clin Invest 1985;76:1713–1719.
25 Kloner RA. Does reperfusion injury exist in humans? J Am Coll Cardiol 1993;21:537–545.
26 Gottlieb RA, Burleson KO, Kloner RA, *et al.* Reperfusion injury induces apoptosis in rabbit cardiomyocytes. J Clin Invest 1994;94:1621–1628.
27 Saraste A, Pulkki K, Kallajoki M, *et al.* Apoptosis in human acute myocardial infarction. Circulation 1997; 95:320–323.
28 Dzau VJ. Predicting the future of human gene therapy for cardiovascular diseases: what will the management of coronary artery disease be like in 2005 and 2010? Am J Cardiol 2003;92:32N–35N.
29 Zhu B, Sun Y, Sievers RE, *et al.* Comparative effects of pretreatment with captopril and losartan on cardiovascular protection in a rat model of ischemia–reperfusion. J Am Coll Cardiol 2000;35:787–795.
30 Novick D, Engelmann H, Wallach D, *et al.* Soluble cytokine receptors are present in normal human urine. J Exp Med 1989;170:1409–1414.
31 Muller-Newen G, Kuster A, Hemmann U, *et al.* Soluble IL-6 receptor potentiates the antagonistic activity of soluble gp130 on IL-6 responses. J Immunol 1998;161: 6347–6355.
32 Oh JW, Revel M, Chebath J. A soluble interleukin 6 receptor isolated from conditioned medium of human breast cancer cells is encoded by a differentially spliced mRNA. Cytokine 1996;8:401–409.
33 Peters M, Jacobs S, Ehlers M, *et al.* The function of the soluble interleukin 6 (IL-6) receptor *in vivo*: sensitization of human soluble IL-6 receptor transgenic mice towards IL-6 and prolongation of the plasma half-life of IL-6. J Exp Med 1996;183:1399–1406.
34 Matsushita K, Umezawa A, Iwanaga S, *et al.* The EAT/mcl-1 gene, an inhibitor of apoptosis, is up-regulated in the early stage of acute myocardial infarction. Biochim Biophys Acta 1999;1472:471–478.
35 El Mouedden M, Laurent G, Mingeot-Leclercq MP, *et al.* Gentamicin-induced apoptosis in renal cell lines and embryonic rat fibroblasts. Toxicol Sci 2000;56: 229–239.
36 Carabello BA. Evolution of the study of left ventricular function: everything old is new again. Circulation 2002;105:2701–2703.
37 Gleason WL, Braunwald E. Studies on the first derivative of the ventricular pressure pulse in man. J Clin Invest 1962;41:80–91.
38 Wallace AG, Skinner Jr NS, Mitchell JH. Hemodynamic determinants of the maximal rate of rise of left ventricular pressure. Am J Physiol 1963;205:30–36.
39 Chen C, Ma L, Linfert DR, *et al.* Myocardial cell death and apoptosis in hibernating myocardium. J Am Coll Cardiol 1997;30:1407–1412.
40 Latif N, Khan MA, Birks E, *et al.* Upregulation of the Bcl-2 family of proteins in end stage heart failure. J Am Coll Cardiol 2000;35:1769–1777.
41 Graeve L, Korolenko TA, Hemmann U, *et al.* A complex of the soluble interleukin-6 receptor and interleukin-6 is internalized via the signal transducer gp130. FEBS Lett 1996;399:131–134.
42 Horsten U, Muller-Newen G, Gerhartz C, *et al.* Molecular modeling-guided mutagenesis of the extracellular part of gp130 leads to the identification of contact sites in the interleukin-6 (IL-6). IL-6 receptor.gp130 complex. J Biol Chem 1997;272:23748–23757.
43 Murakami M, Hibi M, Nakagawa N, *et al.* IL-6-induced homodimerization of gp130 and associated activation of a tyrosine kinase. Science 1993;260:1808–1810.
44 Narazaki M, Witthuhn BA, Yoshida K, *et al.* Activation of JAK2 kinase mediated by the interleukin 6 signal transducer gp130. Proc Natl Acad Sci USA 1994;91: 2285–2289.
45 Ikeda K, Kinoshita M, Tagaya N, *et al.* Coadministration of interleukin-6 (IL-6) and soluble IL-6 receptor delays progression of wobbler mouse motor neuron disease. Brain Res 1996;726:91–97.
46 Hirota H, Yoshida K, Kishimoto T, *et al.* Continuous activation of gp130, a signal-transducing receptor component for interleukin 6-related cytokines, causes myocardial hypertrophy in mice. Proc Natl Acad Sci USA 1995;92:4862–4866.
47 Ikeda K, Iwasaki Y, Tagaya N, *et al.* Neuroprotective effect of cholinergic differentiation factor/leukemia inhibitory factor on wobbler murine motor neuron disease. Muscle Nerve 1995;18:1344–1347.
48 Mitsumoto H, Ikeda K, Holmlund T, *et al.* The effects of ciliary neurotrophic factor on motor dysfunction in wobbler mouse motor neuron disease. Ann Neurol 1994;36:142–148.

49 Leri A, Claudio PP, Li Q, *et al.* Stretch-mediated release of angiotensin II induces myocyte apoptosis by activating p53 that enhances the local renin-angiotensin system and decreases the Bcl-2-to-Bax protein ratio in the cell. J Clin Invest 1998;101:1326–1342.
50 Aikawa R, Komuro I, Yamazaki T, *et al.* Oxidative stress activates extracellular signal-regulated kinases through Src and Ras in cultured cardiac myocytes of neonatal rats. J Clin Invest 1997;100:1813–1821.
51 Slater AF, Stefan C, Nobel I, *et al.* Signalling mechanisms and oxidative stress in apoptosis. Toxicol Lett 1995;82-83:149–153.
52 Gerschenson LE, Rotello RJ. Apoptosis: a different type of cell death. FASEB J 1992;6:2450–2455.
53 Korsmeyer SJ. Regulators of cell death. Trends Genet 1995;11:101–105.
54 Matsushita K, Okita H, Suzuki A, *et al.* Islet cell hyperplasia in transgenic mice overexpressing EAT/mcl-1, a bcl-2 related gene. Mol Cell Endocrinol 2003;203:105–116.
55 Shimizu S, Eguchi Y, Kamiike W, *et al.* Bcl-2 blocks loss of mitochondrial membrane potential while ICE inhibitors act at a different step during inhibition of death induced by respiratory chain inhibitors. Oncogene 1996;13:21–29.
56 Shimizu S, Eguchi Y, Kamiike W, *et al.* Retardation of chemical hypoxia-induced necrotic cell death by Bcl-2 and ICE inhibitors: possible involvement of common mediators in apoptotic and necrotic signal transductions. Oncogene 1996;12:2045–2050.
57 Deten A, Volz HC, Briest W, *et al.* Cardiac cytokine expression is upregulated in the acute phase after myocardial infarction. Experimental studies in rats. Cardiovasc Res 2002;55:329–340.
58 Frangogiannis NG, Youker KA, Rossen RD, *et al.* Cytokines and the microcirculation in ischemia and reperfusion. J Mol Cell Cardiol 1998;30:2567–2576.
59 Kukielka GL, Smith CW, Manning AM, *et al.* Induction of interleukin-6 synthesis in the myocardium. Potential role in postreperfusion inflammatory injury. Circulation 1995;92:1866–1875.
60 Sawa Y, Ichikawa H, Kagisaki K, *et al.* Interleukin-6 derived from hypoxic myocytes promotes neutrophil-mediated reperfusion injury in myocardium. J Thorac Cardiovasc Surg 1998;116:511–517.
61 Ohtsuka T, Hamada M, Inoue K, *et al.* Relation of circulating interleukin-6 to left ventricular remodeling in patients with reperfused anterior myocardial infarction. Clin Cardiol 2004;27:417–420.
62 Hajjar RJ, Schmidt U, Matsui T, *et al.* Modulation of ventricular function through gene transfer *in vivo.* Proc Natl Acad Sci USA 1998;95:5251–5256.
63 Peters M, Blinn G, Solem F, *et al. In vivo* and *in vitro* activities of the gp130-stimulating designer cytokine Hyper-IL-6. J Immunol 1998;161:3575–3581.

MOLECULAR AND CELLULAR BIOLOGY, June 2005, p. 5183–5195 Vol. 25, No. 12
0270-7306/05/$08.00+0 doi:10.1128/MCB.25.12.5183–5195.2005

Combination of hTERT and *bmi-1*, E6, or E7 Induces Prolongation of the Life Span of Bone Marrow Stromal Cells from an Elderly Donor without Affecting Their Neurogenic Potential†

Taisuke Mori,[1,2,3] Tohru Kiyono,[3] Hideaki Imabayashi,[1,4] Yukiji Takeda,[1,2,6] Kohei Tsuchiya,[1] Shunichirou Miyoshi,[5] Hatsune Makino,[1] Kenji Matsumoto,[7] Hirohisa Saito,[7] Satoshi Ogawa,[5] Michiie Sakamoto,[2] Jun-Ichi Hata,[1] and Akihiro Umezawa[1]*

Department of Reproductive Biology and Pathology, National Research Institute for Child Health and Development, Tokyo, Japan[1]; Department of Pathology, Keio University School of Medicine, Tokyo, Japan[2]; Virology Division, National Cancer Center Research Institute, Tokyo, Japan[3]; Department of Orthopedic Surgery, Keio University School of Medicine, Tokyo, Japan[4]; Cardiopulmonary Division, Department of Internal Medicine, Keio University School of Medicine, Tokyo, Japan[5]; Department of General Medicine and Clinical Investigation, Nara Medical University, Nara, Japan[6]; and Department of Allergy and Immunology, National Research Institute for Child Health and Development, Tokyo, Japan[7]

Received 11 January 2005/Returned for modification 13 February 2005/Accepted 14 March 2005

Murine bone marrow stromal cells differentiate not only into mesodermal derivatives, such as osteocytes, chondrocytes, adipocytes, skeletal myocytes, and cardiomyocytes, but also into neuroectodermal cells in vitro. Human bone marrow stromal cells are easy to isolate but difficult to study because of their limited life span. To overcome this problem, we attempted to prolong the life span of bone marrow stromal cells and investigated whether bone marrow stromal cells modified with *bmi-1*, hTERT, E6, and E7 retained their differentiated capability, or multipotency. In this study, we demonstrated that the life span of bone marrow stromal cells derived from a 91-year-old donor could be extended and that the stromal cells with an extended life span differentiated into neuronal cells in vitro. We examined the neuronally differentiated cells morphologically, physiologically, and biologically and compared the gene profiles of undifferentiated and differentiated cells. The neuronally differentiated cells exhibited characteristics similar to those of midbrain neuronal progenitors. Thus, the results of this study support the possible use of autologous-cell graft systems to treat central nervous system diseases in geriatric patients.

Murine and human bone marrow stromal cells differentiate into osteoblasts (2), chondrocytes (13), skeletal myocytes, adipocytes, and cardiomyocytes (24) in vitro and thus are a useful cell source for bone regeneration (26) and in vivo cardiovasculogenesis (11). However, recent studies suggest that bone marrow stromal cells can also differentiate into a neuronal lineage (22), and murine bone marrow-derived multipotent adult progenitor cells differentiate into dopaminergic neuronal cells (16). Since the use of bone marrow stromal cells entails no ethical or immunological problems, and bone marrow aspiration is an established routine procedure, they may be a useful source of cells for transplantation.

Large numbers of cells may be necessary for repairing damaged human tissues to restore function. However, there have been no reports of a sufficient number of differentiated neurons ever having been obtained from human marrow stromal cells. One reason is that normal human cells undergo a limited number of divisions in culture and then enter a nondividing state referred to as "senescence." Senescence is classified into two categories: "stress-induced premature senescence," or "telomere-independent senescence," and "replicative senescence," or "telomere-dependent senescence" (3, 5, 38). $p16^{Ink4a}$ (p16), a cyclin-dependent kinase (CDK) inhibitor, is induced by certain oncogenes and other damage or stress signals and is required for "premature senescence" in human mammary epithelial cells and keratinocytes. p16 inhibits dephosphorylation of pRb by Cdk4/6-cyclin D, and hypophosphorylated pRb actively represses the genes required for the S phase by sequestering the E2F transcription factors. "Replicative senescence" is caused by telomere size reduction during successive cell divisions because of the chromosome end replication problem. Ectopic expression of telomerase alone bypasses replicative senescence in certain cell types, such as human foreskin fibroblasts.

To obtain enough human cells to restore the function of failing organs and to establish a model of cell therapy, the life span of human marrow stromal cells was extended by infecting them with retrovirus encoding human telomerase reverse transcriptase (hTERT) and the human papillomavirus E6 and E7 genes. Both p16/Rb inactivation by E7 and telomerase activation by E6 are required to extend the life span of human

* Corresponding author. Mailing address: Department of Reproductive Biology and Pathology, National Research Institute for Child Health and Development, 2-10-1 Okura, Setagaya-ku, Tokyo 157-8535, Japan. Phone: 81-3-5494-7047. Fax: 81-3-5494-7048. E-mail: umezawa@1985.jukuin.keio.ac.jp.

† Supplemental material for this article may be found at http://mcb.asm.org/.

mammary epithelial cells (21) and umbilical cord blood-derived cells (36). E6 also accelerates the degradation of p53, which induces the CDK inhibitor p21 (35). In contrast to foreskin fibroblasts (5), however, the increase in telomerase activity as a result of the introduction of hTERT is insufficient to prolong the life span of marrow stromal cells (27).

The protocols for in vitro differentiation into neuronal cells include the use of a demethylating agent and/or the neurotrophic cytokines, such as nerve growth factor (NGF), brain-derived neurotrophic factor (BDNF), and neurotrophin 3. Basic fibroblast growth factor (bFGF) activates essential neuronal transcription factors, such as Hes-1 (10), in neural precursor cells and embryonic stem cells (19, 31). The Notch-Hes1 pathway plays an essential role in inhibition of neuronal differentiation (17), and the B27 supplement is effective in achieving long-term viability of primary neurons in culture (7). Taking these findings into consideration, a simple protocol for neural transdifferentiation was developed in this study.

The first purpose of this study was to determine whether prolonging the cell life span with cell cycle-associated molecules would inhibit neurogenic differentiation of marrow stromal cells in vitro. The second purpose was to determine if transdifferentiation of marrow cells of mesodermal origin to neurogenic cells was accompanied by global changes in gene expression or only leaky expression of some neurogenic markers. The in vitro differentiation process appears to be highly specific, and the life span of marrow-derived stromal cells can be extended by retrovirus-mediated transfer of the *bmi-1* gene, which reduces expression of p16 (14, 15, 37), stimulates cell proliferation (9), and is required for maintenance of self-renewing hematopoietic stem cells (29).

MATERIALS AND METHODS

Isolation and cell culture. After signed informed consent was obtained, bone marrow cells were harvested from a 91-year-old human female donor with the approval (approval numbers 13-1 and 12-1) of the Ethics Committee of Keio University School of Medicine. The cells were resuspended in growth medium (MSCGM, PT-3238, and PT-4105; Cambrex Bio Science Walkersville, Inc., Walkersville, MD) and cultured as previously described (1, 13). Several bone marrow stromal cell strains, designated H4-1, H4-2, and H4-3, were generated from primary or first-passage cells using the limiting dilution method. The cells were cultured for further experiments under the approval (approval numbers 25 and 49) of the Ethics Committee of the National Research Institute for Child Health and Development, Tokyo, Japan.

Infection with recombinant retroviruses. The cells were prepared for infection with recombinant retroviruses carrying the *bmi-1*, E6, E7, and hTERT genes, as previously described (1). Stably transduced cells with an expanded life span were designated UBT-5, UBE6T-6, UBE6T-7, UE7T-9, UE6E7T-11, UE6E7T-12, UE7T-13, UBT-15, and UE6E7-16 cells.

Neuronal differentiation of bone marrow stromal cells. Cells removed from the flask bottom were replated onto a coverslip coated with laminin-polylysine (no. 354455; Becton Dickinson BioScience) in MSCGM. One day after passage, the medium was replaced with B27-supplemented Dulbecco's modified Eagle's medium-F12 (Gibco, BRL) containing 20 ng/ml of BDNF (R&D), 10 ng/ml of bFGF (R&D), and 50 ng/ml of NGF (Invitrogen) for neuroectodermal differentiation. Bone marrow stem cells were processed for immunocytochemistry and reverse transcription (RT)-PCR 7 to 21 days after induction.

RT-PCR. Total RNA was prepared from cultured cells with Isogen (Nippon Gene, Tokyo, Japan). Human neuronal RNA was purchased (human total brain RNA; lot 2110667; Becton Dickinson BioScience). RNA for RT-PCR was converted to cDNA with a First-strand cDNA Synthesis kit (Amersham Pharmacia Biotech) according to the manufacturer's recommendations. The following PCR primer sets were used for neuron-associated genes: nestin mRNA, sense (5′-AGAGGGGAATTCCTGGAG-3′) and antisense (5′-CTGAGGACCAGGACTCTCTA-3′); NF-M mRNA, sense (5′-TGAGCTACACGTTGGACTCG-3′) and antisense (5′-TCTCCGCCTCAATCTCCTTA-3′); notch-I mRNA, sense (5′-TCACGCTGACGGAGTACAAG-3′) and antisense (5′-CCACACTCGTTGACATCCTG-3′); Sox-2 mRNA, sense (5′-CACAACTCGGAGATCAGCAA-3′) and antisense (5′-GTTCATGTGCGCGTAACTGT-3′); neuronal cell adhesive molecule (N-CAM) mRNA, sense (5′-TCCATCACCTGGAGGACTTC-3′) and antisense (5′-CTCCAGATAGCTGGCAGAGG-3′); MAP-2 mRNA, sense (5′-GGATTCTGGCAGCAGTTCTC-3′) and antisense (5′-TCCTTGCAGACACCTCCTCT-3′); tubulin-beta III mRNA, sense (5′-ACCTCAACCACCTGGTATCG-3′) and antisense (5′-TGCTGTTCTTGCTCTGGATG-3′); and Nur-related factor-1 (Nurr1) mRNA, sense (5′-TTTCTGCCTTCTCCTGCATT-3′) and antisense (5′-GTGGCACCAAGTCTTCCAA-3′); 18S mRNA sense (5′-GTGGAGCGATTTGTCTGGTT-3′) and antisense (5′-CGCTGAGCCAGTCAGTGTAG-3′) were used as a positive control. PCR was performed with TaKaRa Z-Taq (TAKARA SHUZO Co., Ltd.) for 30 cycles, with each cycle consisting of 98°C for 5 s, 68°C or 60°C for 1 s, and 72°C for 10 s, with an additional 30-s incubation at 72°C after completion of the final cycle.

Western blot analysis. To detect p16, p53, p21, p27, Rb, Bmi-1, and actin, immunoblotting was performed as previously described (30) with antibodies against p16 (G3-245; BD Pharmingen, San Diego, CA), Rb (G174-405; BD Pharmingen), p53 (DO-1), p21 (Ab-1; Oncogene Science, Boston, MA), Bmi-1 (monoclonal antibody generated by T. Kiyono), p27 (BD Pharmingen), and actin (Santa Cruz Biotechnology Inc., Santa Cruz, CA).

Telomere length assay. Genomic DNA was extracted from cultured cells. Restriction enzyme digestion of genomic DNA was carried out with HinfI and RsaI. The fragments obtained were resolved on 0.7% agarose gels, transferred to a Hybond N membrane (Amersham, United Kingdom), and hybridized with digoxigenin-labeled $(TTAGGG)_3$ probe. The membrane was then incubated with anti-digoxigenin alkaline phosphatase, and detection was performed with a chemiluminescence solution. The size range and intensity were determined with X-ray film.

Telomerase activity analysis. Telomerase activity was determined with a telomere repeat amplification protocol (TRAP) assay kit, Telo TAGGG telomerase PCR ELISA plus (Roche, Indianapolis, IN), according to the manufacturer's instructions.

G-banding karyotypic analysis. Metaphase spreads were prepared from cells treated with Colcemid (Karyo Max; Gibco BRL; 100 ng/ml for 6 h). We performed a standard G-banding karyotypic analysis on at least 50 metaphase spreads for each population.

SKY analysis. Spectral karyotyping (SKY) was performed on metaphase-transduced cells (UBE6T-7, UE6E7T12, and UE7T13) in 80 population doublings (PDs) according to the kit manufacturer's instructions (ASI, Carlsbad, CA) and a previously published method (34).

Immunocytochemical analysis. Immunocytochemical analysis was performed as previously described (30) with antibodies to MAP-2 (Zymed, San Francisco, CA), tubulin 3 (Sigma, St. Louis, Missouri), GFAP (DAKO, Denmark), Nurr1 (N-20; Santa Cruz), and nestin (Biogenesis, United Kingdom) in phosphate-buffered saline containing 1% bovine serum albumin. As a methodological control, the primary antibody was omitted. After being washed in phosphate-buffered saline, the slides were incubated with fluorescein isothiocyanate-conjugated anti-mouse immunoglobulin antibody or phycoerythrin (PE)-conjugated anti-rabbit immunoglobulin antibody (DAKO, Denmark).

GeneChip expression analysis. Human genomewide gene expression was examined with the Human Genome U133A Probe array (GeneChip; Affymetrix), which contains the oligonucleotide probe set for approximately 23,000 full-length genes and expressed sequence tags, according to the manufacturer's protocol (Expression Analysis technical manual and GeneChip Small Sample Target Labeling Assay version 2 technical note [http://www.affymetrix.com/support/technical/index.affx]). Total RNA was isolated with an RNeasy minikit (QIAGEN, Chatsworth, CA). Double-stranded cDNA was synthesized, and the cDNA was subjected to in vitro transcription in the presence of biotinylated nucleoside triphosphates. The biotinylated cRNA was hybridized with a probe array for 16 h at 45°C, and the hybridized biotinylated cRNA was stained with streptavidin-PE and scanned with a Hewlett-Packard Gene Array Scanner. The fluorescence intensity of each probe was quantified by using the GeneChip Analysis Suite 5.0 computer program (Affymetrix). The expression level of a single mRNA was determined as the average fluorescence intensity among the intensities obtained with 11 paired (perfectly matched and single-nucleotide-mismatched) probes consisting of 25-mer oligonucleotides. If the intensities of mismatched probes were very high, gene expression was judged to be absent, even if high average fluorescence was obtained with the GeneChip Analysis Suite 5.0 program. The level of gene expression was determined with the GeneChip software as the average difference (AD). Specific AD levels were then calculated as percentages of the mean AD level of six probe sets for housekeeping genes (actin and GAPDH [glyceralde-

hyde-3-phosphate dehydrogenase] genes). Further data analysis was performed with Genespring software version 5 (Silicon Genetics, San Carlos, CA). To normalize the staining intensity variations among chips, the AD values for all genes on a given chip were divided by the median of all measurements on that chip. To eliminate changes within the range of background noise and to select the most differentially expressed genes, data were used only if the raw data values were less than 100 AD and gene expression was judged to be present by the Affymetrix data analysis. Hierarchical clustering analysis with standard correlation was used to identify gene clusters. The separation ratio was set at 0.5. Normalization values were considered significant when (i) expression changed by at least twofold (activation program) and (ii) increased gene expression included at least one present absolute call (Affymetrix algorithm). Normalized values were averaged for two donors and used for the data analysis, and the normalized values were used to classify the genes into up-regulated or down-regulated. There was a statistically significant correlation between the expression levels of genes of the same cells analyzed twice ($r = 0.997$). These criteria confirmed the reproducibility of the differences that were seen between different cells under different conditions.

Calcium imaging. The intracellular Ca^{2+} concentration was monitored by means of the fluorescent Ca^{2+} indicator Fluo-3. The cultured cells were exposed to 10 μmol/liter Fluo-3 acetoxymethylester (Molecular Probes, Eugene, Oregon) at 37°C for 30 min and then washed in Tyrode's solution containing (in mmol/liter) NaCl, 140; KCl, 4; $MgCl_2$, 0.5; $CaCl_2$, 1.8; HEPES, 5; and D-glucose, 55 (pH adjusted to 7.4 with NaOH). The signal from the cell was monitored with a fluorescence microscope (BX50WI; Olympus, Tokyo, Japan) and a high-resolution optical mapping system (MiCAM-01; SciMedia Ltd. Tokyo, Japan) at a wavelength of 530 nm and an excitation wavelength of 488 nm. The cells were challenged with a depolarization stimulus in the form of high-potassium (144 mmol/liter) Tyrode's solution (KCl substituted for NaCl) applied with a rapid solution changer (RSC-160; Molecular Kinetics, Indianapolis, Indiana) at a flow rate of 100 μl/s at a distance of 1 mm from the cell at a room temperature of 25°C. The image analysis was performed with Igor Pro software (Wavemetrics, Lake Oswego, OR) and by customized procedures. The background fluorescence intensity was subtracted from the data, and the areas were normalized to the control response to normal Tyrode's solution and shown on a color scale.

Quantitative RT-PCR. RNA was extracted from cells using the RNeasy kit (QIAGEN, Valencia, CA). Contaminating DNA was eliminated by two sequential DNase (Invitrogen) treatments. An aliquot (1 μg) of total RNA was reverse transcribed by using an oligo(dT) primer. For the thermal cycle reactions, cDNA was amplified (ABI PRISM 7000; Perkin-Elmer Applied Biosystems) using the SYBR RT-PCR kit (Takara Bio, Japan) under the following reaction conditions: 40 cycles of PCR (95°C for 15 seconds and 60°C for 1 min) after an initial denaturation (95°C for 10 min). The controls consisted of amplifications without reverse transcription and reactions without the addition of a cDNA template. The authenticity and sizes of the PCR products were confirmed using a melting curve analysis (using software provided by Perkin-Elmer) and a gel analysis. mRNA levels were normalized using the GAPDH gene as a housekeeping gene. The following primer sets were used: hTERT mRNA, sense (5′-CGGTGTGC ACCAACATCTACAAG-3′) and antisense (5′-TCAGAGATGACGCGCAGG A-3′); Bmi-1 mRNA, sense (5′-CGCTTGGCTCGCATTC-3′) and antisense (5′-AGCTCAGTGATCTTGATTCTCGTTG-3′); E6 mRNA, sense (5′-GCACAG AGCTGCAAACAACT-3′) and antisense (5′-CTCACGTCGCAGTAACTGTT G-3′); E7 mRNA, sense (5′-ATGACAGCTCAGAGGAGGAG-3′) and antisense (5′-TCCTAGTGTGCCCATTAACAG-3′); NR4A2/Nurr1 mRNA, sense (5′-TTCGGCAGAGTTGAATGAATG-3′) and antisense (5′-GAAATTAAAG GTGGACAGTGTCGTA-3′); and GAPDH mRNA, sense (5′-CCAGCCGAG CCACATCGCTC-3′) and antisense (5′-ATGAGCCCCAGCCTTCTCCAT-3′).

Nucleotide sequence accession numbers. The gene chip datasets have been deposited in the GEO database with accession number GSE2110 (GSM38114 to GSM38116).

RESULTS

Human marrow stromal cells with an extended life span. Bone marrow stromal cells were obtained from a 91-year-old human donor and subcloned by limiting dilution. One subclone of the cells isolated was designated H4-1 cells (Fig. 1). To extend the life span of the H4-1 cells and obtain a large number of cells, five different types of cells were obtained by transducing them with combinations of *bmi-1*, E6, E7, and/or TERT genes (http://1985.jukuin.keio.ac.jp/umezawa/cells/name.html). We referred to the cells transduced with *bmi-1* and TERT as UBT-5 and UBT-15 cells, the cells transduced with *bmi-1*, E6, and TERT as UBE6T-6 and UBE6T-7 cells, the cells transduced with E7 and TERT as UE7T-9 and UE7T-13 cells, the cells transduced with E6, E7, and TERT as UE6E7T-11 and UE6E7T-12 cells, and the cells transduced with E6 and E7 as UE6E7-16 cells. Random amplified polymorphic DNA analysis revealed that the five different types of stable transduced cells (UBT-5, UBE6T-7, UE6E7T-12, UE7T-13, and UE6E7-16) were definitely derived from H4-1 cells (see Fig. S1 in the supplemental material).

The UE6E7T-12, UE6E7T-11, UE7T-9, UE7T-13, UBE6T-6, and UBE6T-7 cells were successfully grown and were shown to have extended life spans (Fig. 1A). The life spans of the UE6E7T-12 and UE7T-13 cells were extended to 200 PDs. The life spans of the UBT-5, UBE6T-7, UE6E7T-11, UE7T-9, and UBE6T-6 cells were extended to 60 PDs. The UBT-5 cells also proliferated for more than 60 PDs and were shown to have an extended life span. However, hTERT alone did not extend the life span (data not shown). Nontransduced parental H4-1 cells reached "senescence" in culture at 44 PDs, and UE6E7-16 cells entered a period of "crisis" in culture at 70 PDs (Fig. 1A and B), implying that E6 and E7 are able to prolong the cell life span but that their prolonging effect is limited. The H4-1 cells exhibited large, flat morphology at 40 PDs, while the other cells were small and spindle shaped (Fig. 1C).

None of the cells exhibited malignant transformation activity: they did not form a focus after confluence in vitro; cells grafted into subcutaneous tissue of immunodeficient mice (nonobese diabetic [NOD]-SCID-interleukin 2 receptor knockout mice) did not form tumors, at least during the observation period (more than 30 days); and the morphologies of all clones remained unchanged for 40 to 200 PDs.

Expression of Bmi-1, Rb, p53, p27, and p21 proteins in transduced cells. The expression of cell cycle-associated proteins was analyzed in cells transduced with the hTERT and *bmi-1*, E6, or E7 genes and in parental H4-1 cells (Fig. 2). Human dermal keratinocytes at senescence (PD 27) served as a control for expression of $p16^{Ink4a}$, hypophosphorylated RB, and p53 proteins at a high level.

Bmi-1 proteins were expressed in the UBT-5 and UBE6T-7 cells, but not in the H4-1, UE6E7-12, and UE7T-13 cells. p16 proteins were down-regulated in the *bmi-1*-overexpressing cells, i.e., UBT-5 and UBE6T-7 cells. p53 and p21 proteins were down-regulated in E6-overexpressing UBE6T-7 and UE6E7T-12 cells. These results are consistent with the hypothesis that p53 is proteolysed via ubiquitination by E6 (33). Hypophosphorylated Rb was down-regulated in E7-overexpressing cells, probably as a result of proteolysis by E7. There was no significant difference in p27 protein levels between any of the cells tested.

Increase in telomerase activity and maintenance of telomere length in cells transduced with the hTERT gene. No telomerase activity was detected by the TRAP assay in the parental H4-1 cells at PDs 20 and 40, but telomerase activity was detected in UBT-5, UBE6T-7, UE6E7T-12, and UE7T-13 cells transduced with the hTERT gene at all of the PDs tested. UE6E7-16 cells not transduced with the hTERT gene did not exhibit any telomerase activity at PDs 40 to 120 (Fig. 3A). Likewise, the telomere length of the parental H4-1 cells decreased with the number of PDs, whereas the telomere length